PERGAMON

Continental Shelf Research 22 (2002) 719–748

CONTINENTAL SHELF RESEARCH

www.elsevier.com/locate/csr

West Florida shelf circulation and temperature budget for the 1999 spring transition

Ruoying He, Robert H. Weisberg*

College of Marine Science, University of South Florida, 140 7th Ave. South, St. Petersburg, FL 33701, USA

Received 26 February 2001; received in revised form 31 August 2001; accepted 7 September 2001

Abstract

Mid-latitude continental shelves undergo a spring transition as the net surface heat flux changes from cooling to warming. Using in situ data and a numerical circulation model we investigate the circulation and temperature budget on the West Florida Continental Shelf (WFS) for the spring transition of 1999. The model is a regional adaptation of the primitive equation, Princeton Ocean Model forced by NCEP reanalysis wind and heat flux fields and by river inflows. Based on agreements between the modeled and observed fields we use the model to draw inferences on how the surface momentum and heat fluxes affect the seasonal and synoptic scale variability. We account for a strong southeastward current at mid-shelf by the baroclinic response to combined wind and buoyancy forcing, and we show how this local forcing leads to annually occurring cold and low salinity tongues. Through term-by-term analyses of the temperature budget we describe the WFS temperature evolution in spring. Heat flux largely controls the seasonal transition, whereas ocean circulation largely controls the synoptic scale variability. These two processes, however, are closely linked. Bottom topography and coastline geometry are important in generating regions of convergence and divergence. Rivers contribute to the local hydrography and are important ecologically. Along with upwelling, river inflows facilitate frontal aggregation of nutrients and the spring formation of a high concentration chlorophyll plume near the shelf break (the so-called 'Green River') coinciding with the cold, low salinity tongues. These features originate by local, shelf-wide forcing; the Loop Current is not an essential ingredient.

Keywords: Circulation; Temperature budget; West Florida shelf; Modeling and observations

1. Introduction

Located at the eastern edge of the Gulf of Mexico, the West Florida Continental Shelf (WFS) is one of the broadest continental shelves in North America. Between its southern and northern ends, bounded by the Florida Keys and the Florida Big Bend, respectively, the WFS isobaths vary smoothly, and they generally parallel the coastline. This geometry changes along the Florida Panhandle in the north where the coastline undergoes a right angle bend, and the shelf width decreases to a minimum at the DeSoto Canyon.

Long-term observations (Weisberg et al., 1996) show that the WFS circulation, forced by tides, winds, buoyancy, and possible interactions with the Gulf of Mexico Loop Current, varies on time

*Corresponding author. Tel.: +1-727-553-1568; fax: +1-727-553-1189.

E-mail address: weisberg@marine.usf.edu (R.H. Weisberg).

0278-4343/02/$ - see front matter
PII: S0278-4343(01)00085-1

scales from semi-diurnal to inter-annual. Monthly mean currents at mid-shelf suggest a seasonal cycle with along-shore flows either to the southeast in spring, or to the northwest in late summer to early autumn. Weisberg et al. (1996) hypothesized that these seasonal currents are of a baroclinic nature based on an observed thermal wind shear and the seasonal reversal of the across-shelf density gradient. As a consequence of the spring transition in surface heat flux from cooling to warming, they argued that spatial differences in heating (from the coast to offshore by increasing depth and from the south to north by solar declination) forms a mid-shelf cold tongue and a seasonally maximum across-shelf density gradient that supports a southeastward current. Here we examine this locally forced, seasonal circulation hypothesis by focusing on the spring transition for 1999, a year when the Loop Current, as evidenced in relatively flat isopycnal topography at the shelf break, did not have a strong direct influence on the WFS. Our objective is to describe the circulation and temperature budget for spring 1999 with respect to the shelf-wide winds, surface heat fluxes, and river inflows.

An argument used to describe the transition from wintertime horizontal stratification to summertime vertical stratification for mid-latitude shelves is that decreased winds and increased solar heating conspire to form a thermocline. The details of this process are not well understood, however. Chapman and Gawarkiewicz (1993) reason that nonlinearity in the equation of state can account for the elimination of horizontal stratification by spatially uniform heating, but Morey (1999) point out that this argument is valid only for certain salinity and temperature ranges. Other processes must also be important. Morey (1999), using a two-dimensional model with a sloping bottom, argue that the surface heat flux divided by the water depth is the critical factor in the seasonal transition, essentially the differential heating argument advanced earlier. The degree to which their argument is valid in the fully three-dimensional sense and the regional partition between ocean dynamical and local heating affects are also topics of our paper.

The observational record (e.g. Niiler, 1976; Mitchum and Sturges, 1982; Cragg et al., 1983; Marmorino, 1983a, b; Mitchum and Clarke, 1986b) shows that the WFS circulation and sea level variations are highly correlated with the synoptic scale wind stress variations. The passage of cold fronts also affects the local temperature balance (e.g., Price, 1976). Along with these local synoptic scale variations are baroclinic effects that originate with the Loop Current at the shelf break (e.g., Paluszkiewicz et al., 1983). What remains unclear are the relative importance between the momentum and buoyancy that are input either locally, or at the shelf break.

Such questions are of multi-disciplinary interest since, despite its oligotrophic description, the WFS supports highly productive ecosystems. These include episodic toxic dinoflagellate blooms (red tides) near the coast (Steidinger, 1983; Vargo et al., 1987), a seasonal chlorophyll plume near the shelf break (Gilbes et al., 1996), and important commercial and recreational fisheries throughout the WFS. Parallel programs of in situ measurements and numerical model experiments are presently in place for an improved understanding of the circulation and how it affects seasonally varying water properties and influences organism growth and distribution.

This paper focuses on local wind and buoyancy forcing during the spring transition of 1999, independent of the Loop Current. We use the primitive equation, Princeton ocean model (POM) described by Blumberg and Mellor (1987) forced by National Center for Environmental Predication (NCEP) reanalysis winds and net surface heat flux and by river inflows. The only role of the adjacent Gulf of Mexico is to set the vertical distribution of temperature and salinity for initializing the model density field. Once begun, the integration proceeds solely on the basis of local forcing. By running twin experiments, one with heat flux and the other without, we explore the relative importance of wind and buoyancy in effecting the seasonal and synoptic scale variability.

Section 2 describes the model and forcing fields. Section 3 compares model results with in situ observations. Based upon these comparisons, the model is used in Section 4 to describe the seasonal

mean circulation on the WFS for spring 1999 and the evolution of the corresponding temperature and salinity fields. Section 5 presents a term-by-term analysis of the three-dimensional temperature budget. The results are summarized and discussed in Section 6.

2. Model and forcing fields

2.1. Model

We use the POM for the following reasons. First, it has an embedded turbulence closure sub-model (Mellor and Yamada, 1974, 1982; Galperin et al., 1988) for parameterizing vertical turbulence mixing. Second, it employs a sigma coordinate in the vertical which, with the turbulence closure sub-model, is well suited to study the nonlinear dynamics over a shallow, gently sloping continental shelf. Third, its orthogonal curvilinear coordinates in the horizontal are convenient for resolving the near-shore regions.

Previous WFS POM applications include Yang et al. (1999a,b), Li and Weisberg (1999a, b), Weisberg et al. (2000), and Weisberg et al. (2001). Yang et al. (1999a) studied the WFS response to climatological monthly mean wind forcing. Qualitative agreements were found between the model and observations to some extent, but monthly mean wind stress alone could not account for the southeastward current observed at mid-shelf in spring (Weisberg et al., 1996). Li and Weisberg (1999a, b) focused on synoptic scale winds, respectively describing the kinematics and dynamics of WFS responses to idealized upwelling favorable wind forcing under constant density. The inner-shelf length scale was found to be a frictional one, consistent with the analytical work of Mitchum and Clarke (1986a). The same model was also applied to a specific upwelling case study with both constant density and stratified conditions (Weisberg et al., 2000). A comparison of in situ data with model results confirmed a simple Ekman-geostrophic route to spin-up and identified regional upwelling centers promoted by coastline and isobath geometries. The utility of this model in replicating the longer-term synoptic scale variability and the sensitivity of the WFS response to its background density state was then shown by Weisberg et al. (2001). An asymmetry in the inner-shelf responses to upwelling and downwelling favorable winds was found that helps to clarify the scale of the inner-shelf response. Consistent with Ekman dynamics, the inner shelf is the region with divergent bottom boundary layer. Since thermal wind effects can either enhance or decrease the bottom boundary layer development, the inner-shelf under stratified conditions can respond asymmetrically to upwelling and downwelling favorable winds.

Many WFS circulation questions remain. For instance, the relative effects of buoyancy and wind forcing have not been considered. While previous drifter and current meter measurements hint at seasonally varying circulation patterns (Tolbert and Salsman, 1964; Gaul, 1967; Williams et al., 1967; Weisberg et al., 1996; Yang et al., 1999b), there are no definitive measures of these. The communication of water between the deep ocean and the shelf and the communication of water between different regions of the shelf remain poorly understood. To address these questions it is necessary to explore a broader region and consider more complete forcing functions than in previous studies.

The model domain (Fig. 1) extends from the Florida Keys in the southeast to west of the Mississippi River in the northwest, and it has one open boundary arcing between these two locations for which a radiation boundary condition (Orlanski, 1976) is used. The model domain includes the major rivers that impact the WFS and the Desoto Canyon region where the shelf is narrowest, and its orthogonal curvilinear grid has horizontal resolution that varies from less than 2 km near the coast to 6 km near the open boundary. Vertically, the sigma coordinate has 21 layers with higher resolution near the surface and bottom to better resolve the frictional boundary dynamics. In total, the model has $121 \times 81 \times 21$ grid points. Horizontal diffusivities are parameterized using the Smagorinsky (1963) formulation with a coefficient of 0.2. Bottom stress, τ_b, is calculated by a quadratic law with variable drag coefficient having a minimum value

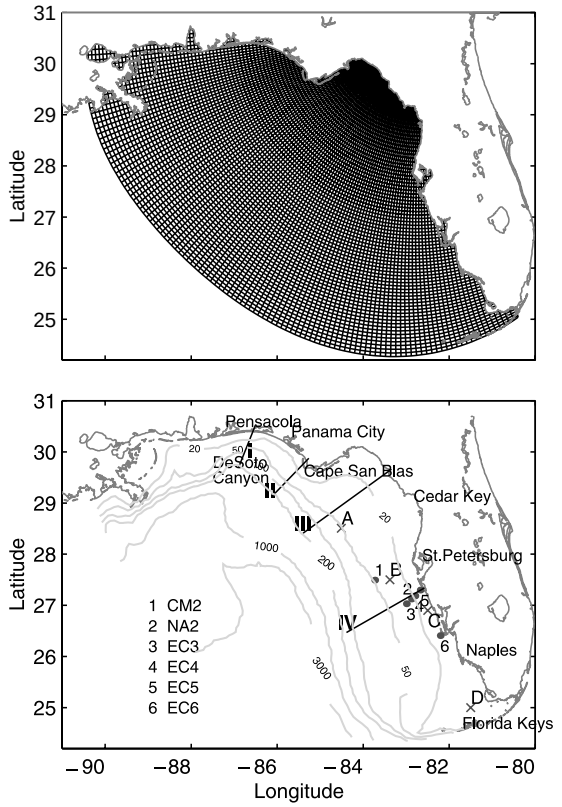

Fig. 1. The regional model grid (upper panel) and bathymetry and station locations (lower panel). Sea level comparisons are with Florida tide gauges at Pensacola, Apalachicola, St. Petersburg, and Naples. Velocity comparisons are with acoustic Doppler current profiles from instruments moored at the 50, 30, 25, 20, and 10 m isobaths (1–6). Temperature is described along transects I–IV, and the temperature budget is diagnosed at Stations A, B, C, and D.

of 0.0025. A mode splitting technique is used for computational efficiency (Blumberg and Mellor, 1987). Here, we use external and internal time steps of 6 and 360 s, respectively.

The model is initialized at rest with horizontally uniform stratification. Stratification above 200 m is based on temperature and salinity observations taken during a March 1999 trans-shelf hydrographic survey [from the Ecology of Harmful Algal Blooms (ECOHAB) Program]. Stratification below 200 m is based on climatology. From this initial zero-baroclinicity state, the model spins up rapidly, generating baroclinicity in balance with the wind and buoyancy forcing. An alternative is to begin with a baroclinic field and allow the model currents to come into balance diagnostically with this field before proceeding with the spring simulation. The hydrographic data are not sufficient for this, however, and spurious currents due to incorrect density would corrupt the experiment. Consistent with our objective of determining the WFS responses to local, shelf-wide forcing only, our initial baroclinicity-free state is a sensible choice.

Tidal forcing is excluded in the present application since we are not considering high frequency variability. It is recognized that tidal mixing can affect the synoptic and seasonal scales when the tidal currents are large, but here the tidal currents are only a few cm s^{-1}. Modeled and observed tidal current analyses will be reported on separately.

2.2. Atmospheric forcing

Different from previous WFS model studies that considered wind forcing only, here we include both wind and thermohaline forcing. The wind and heat flux fields are from the NCEP daily reanalysis product for the period February 28, 1999–June 1, 1999. These values, with a grid resolution of $2.5^\circ \times 2.5^\circ$, are interpolated onto the model grid. The NCEP winds agree well with in situ buoy winds for the spring 1999 season. Unlike the winds, however, coarse resolution renders the NCEP heat flux unrealistic because of smaller scale WFS temperature structures. We correct for this using a relaxation method (e.g., Ezer and Mellor, 1992; Chu et al., 1999). Thus, the surface heat flux forcing is given by

$$K_H \frac{\partial \theta}{\partial z} = \left(\frac{Q_H}{\rho C_P}\right) + C(\theta_{obs} - \theta),$$

$$K_H \frac{\partial S}{\partial z} = 0, \qquad (1)$$

where Q_H is the net heat flux, θ_{obs} is an interpolation of the monthly mean satellite observed sea surface temperature, and C_p is the specific heat. The salinity flux in this study is set to be zero. The relaxation coefficient, C, or the

reciprocal of the restoring time per unit area, is set at 1 m/day. Such relaxation prevents deviations from observed monthly mean SST in an attempt to force realistic baroclinic flow structures. These structures are facilitated by turbulence mixing through the coefficients K_M and K_H computed with the Mellor and Yamada (1982) 2.5 level turbulence closure sub-model.

2.3. Lateral boundary forcing

Gulf of Mexico Loop Current forcing is excluded in this study for two reasons. First, previous observations and model studies concluded that persistent forcing of the middle and inner-shelf by the Loop Current is minimal (Marmorino, 1983a, b, 1982). Second, modeling the effects on the WFS of an aperiodically varying Loop Current and its associated eddies (e.g., Sturges and Leben, 2000) remains a great challenge (Marmorino, 1982; Cooper, 1987), presupposing that the Loop Current itself is being described properly. To better assess the role of the Loop Current as a WFS boundary condition it will be necessary to nest a regional model with a larger Gulf of Mexico/Caribbean/Atlantic Ocean model. This is beyond the scope of the present paper that focuses on local, shelf-wide forcing only. We find, however, that local forcing is capable of driving much of the observed synoptic and seasonal scale variability.

Seven major rivers are introduced into the model domain for land derived buoyancy forcing. These are the Mississippi, Mobile, Apalachicola, Suwannee, Hillsborough, Peace and Shark rivers. We use the technique of Kourafalou et al. (1996) (also see Pullen, 2000), whereby interpolated monthly mean mass flux data for these rivers are input to the top sigma level at the grid cells closest to the rivers' locations.

We define the spring season here as March 1–May 31, and we focus on this period for 1999. As an initial value problem we begin from a state of rest on February 28. With no initial baroclinicity the spin-up phase proceeds rapidly over the course of a few pendulum days, consistent with the barotropic response arguments for a gently sloping shelf of Clarke and Brink (1985). Under the conditions of surface cooling that occurs prior to the spring warming transition in mid-March, convective mixing very efficiently adjusts the initial density field on the shallow shelf. In other words, the "memory" of initial density field for this spring transition experiment is short, and sensitivity experiments that we performed using longer spin-up times showed very little difference from the present model results.

3. Model and data comparisons

3.1. Sea level

Since the model is forced without tides, all of the model and data comparisons are shown after low-pass filtering to exclude tidal and inertial period oscillations. Sea surface height comparisons are given in Fig. 2 at four different tide-gauge stations from Pensacola in the northwest to Naples in the southeast. Agreement is good at all of these with squared correlation coefficients exceeding 0.80. We conclude that coastal sea level for this three-month period responds primarily to local, shelf-wide forcing.

3.2. Currents

Comparisons are made between the modeled and observed velocity vector time series at the 50, 30, 25, 20, and 10 m isobaths (moorings CM2, EC3, NA2, EC4, EC5, and EC6 in Fig. 1). As examples, we show the modeled and observed vector time series at the 50, 25, and 10 m locations in Figs. 3–5, respectively. The observations are from acoustic Doppler current profilers (ADCP), and for each location we show comparisons at three different depths: near-surface, mid-water column, and near-bottom. These comparisons are quantified by a complex correlation analysis (e.g., Kundu, 1976). Defining the modeled and observed velocity vectors in the Argand plane as $w_1 = u_1 + \mathrm{i}v_1$ and $w_2 = u_2 + \mathrm{i}v_2$, respectively, the complex squared correlation coefficient is

$$\rho(w_1, w_2) = \frac{[\overline{w_1^*(t)w_2(t)}]^2}{\overline{[w_1^*(t)w_1(t)]}\,\overline{[w_2^*(t)w_2(t)]}}, \qquad (2)$$

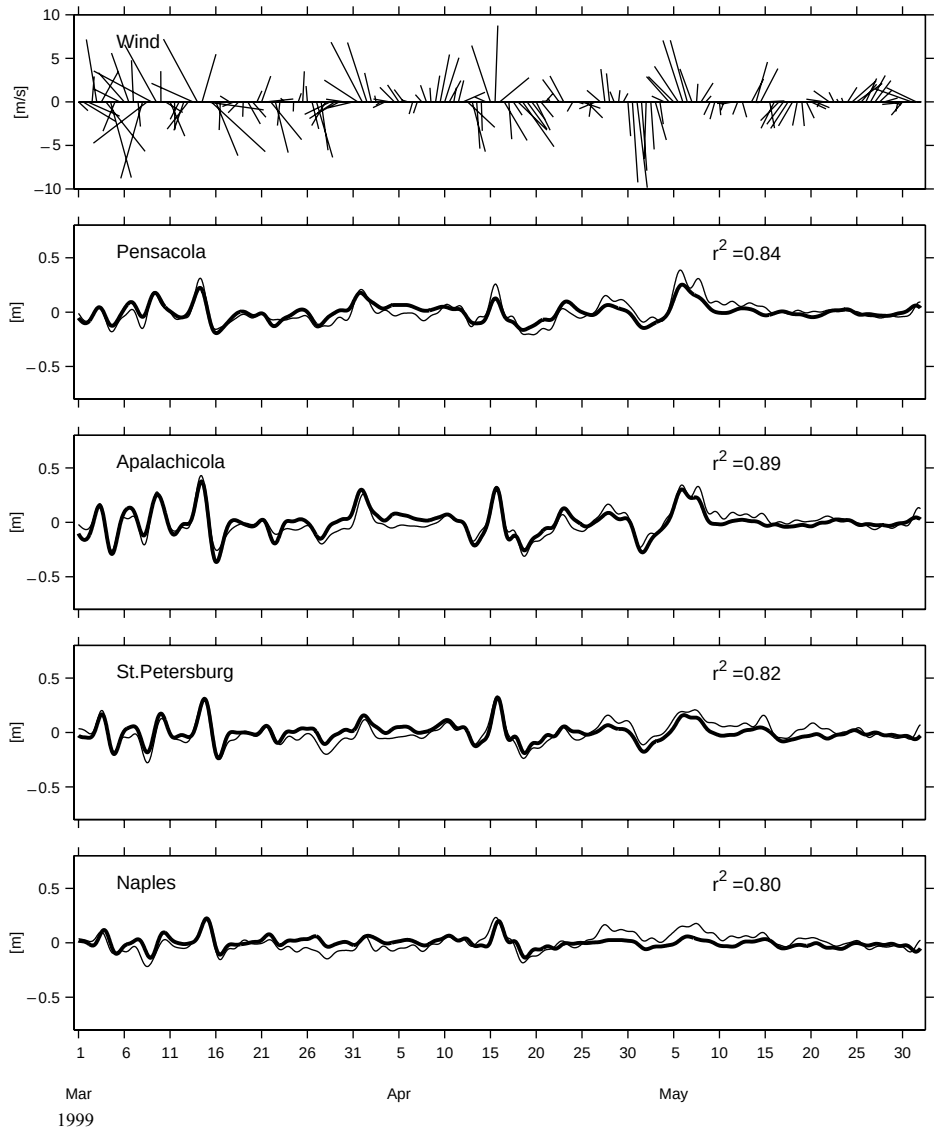

Fig. 2. Comparisons between modeled (bold) and observed (thin) sea level at Pensacola, Apalachicola, St. Petersburg, and Naples as quantified by a squared correlation coefficient, along with the NCEP wind velocity sampled at station A.

where the overbar denotes a time average. The complex correlation has an amplitude and a phase, the amplitude being the correlation coefficient and the phase being the angle (measured counter-clockwise) between the modeled and the observed currents. Like sea level, the modeled and observed currents also compare well as measured by the two sets of numbers provided with each plot. The left-hand sets are the seasonal mean east and north velocity components. The right-hand sets are the squared correlation coefficient, phase angle, and regression coefficient. At all stations and depths the squared correlation coefficients range between 0.62 and 0.82, and the orientations agree to within -10° to $+20^{\circ}$. More importantly, as seen directly from the time series, the model gets the sense of the

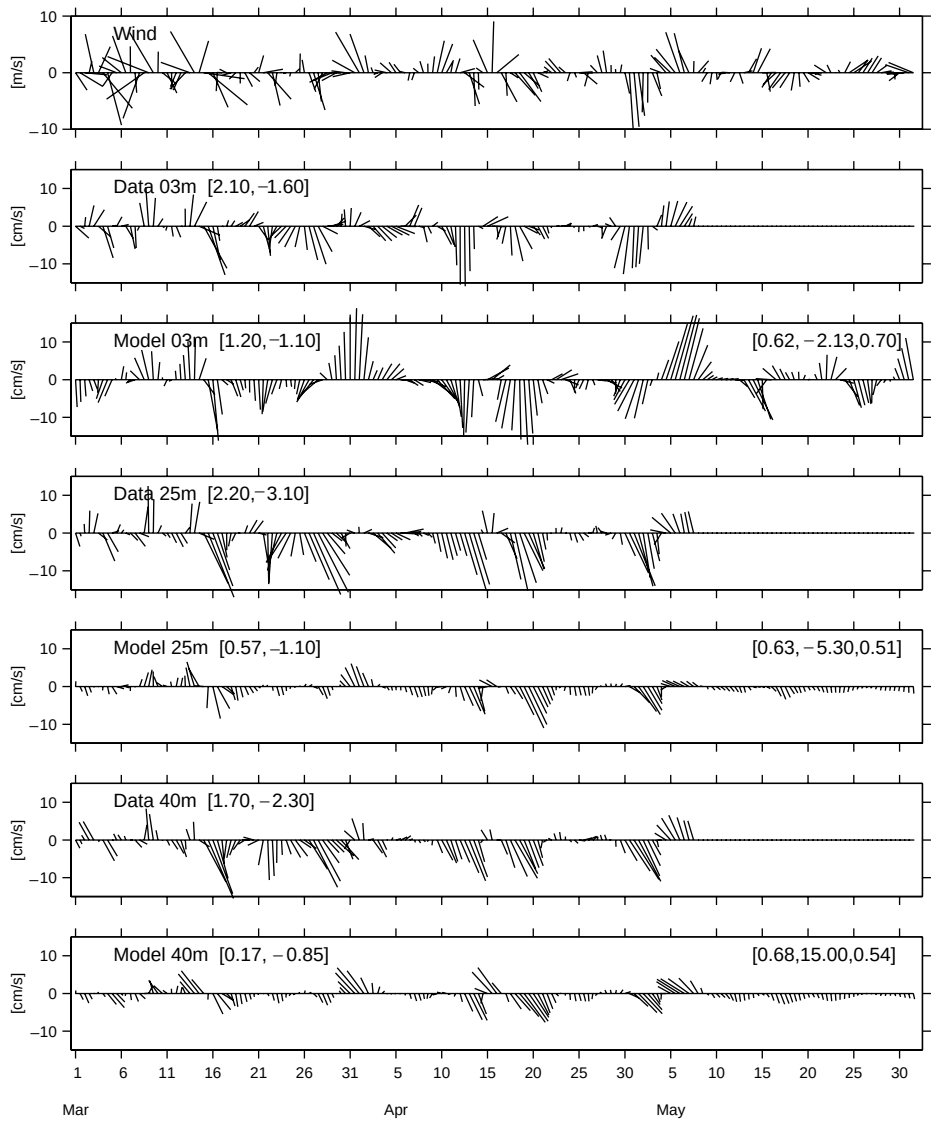

Fig. 3. Comparisons between modeled and observed currents at the 50 m isobath (mooring CM2) sampled at depths of 3, 25 and 40 m, along with the NCEP wind velocity sampled at station A. Each vector current time series is accompanied by its seasonal mean east and north velocity components (left-hand couplet), and each model/data comparison is quantified by its squared complex correlation coefficient, phase angle (or angular deviation of the model vector from the data vector measured counterclockwise), and regression coefficient (right-hand triplet).

velocity rotation correct in both the surface and bottom Ekman layers. A deficiency in the modeled currents, however, lies in the amplitudes. The regression coefficients show that the model underestimates the observed velocity fluctuations by between 20 and 50 percent.

Notwithstanding the amplitude disparity, the model reproduces the patterns of current variability reasonably well. The systematic underestimate of the currents may be the result of the low resolution NCEP forcing fields, and hence too much smoothing when interpolating these fields

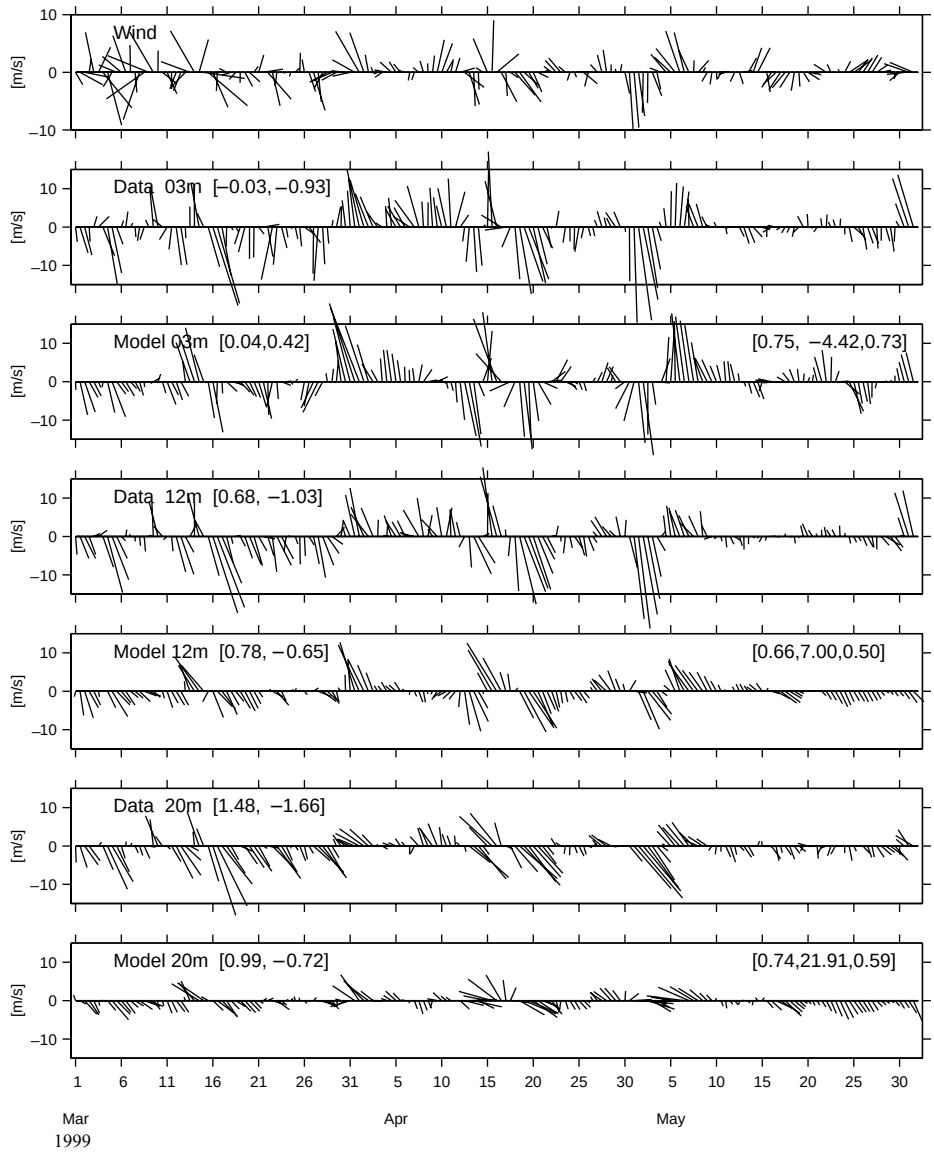

Fig. 4. Comparisons between modeled and observed currents at the 25 m isobath (mooring NA2) sampled at depths of 3, 12, and 20 m, along with the NCEP wind velocity sampled at station A. Quantitative comparisons are as in Fig. 3.

onto the model grid. Model performance also degrades between the shallowest and deepest comparison sites, i.e., the 10 m isobath currents agree better than the 50 m isobath currents. This is expected based on the frictional scale of the inner-shelf response to wind forcing (e.g., Weisberg et al., 2001). The 50 m isobath is at the outer half of the inner-shelf so we anticipate a decreased correlation there.

The modeled and observed velocity comparisons are summarized in Fig. 6 where we show the mid-depth seasonal mean vectors and hodograph

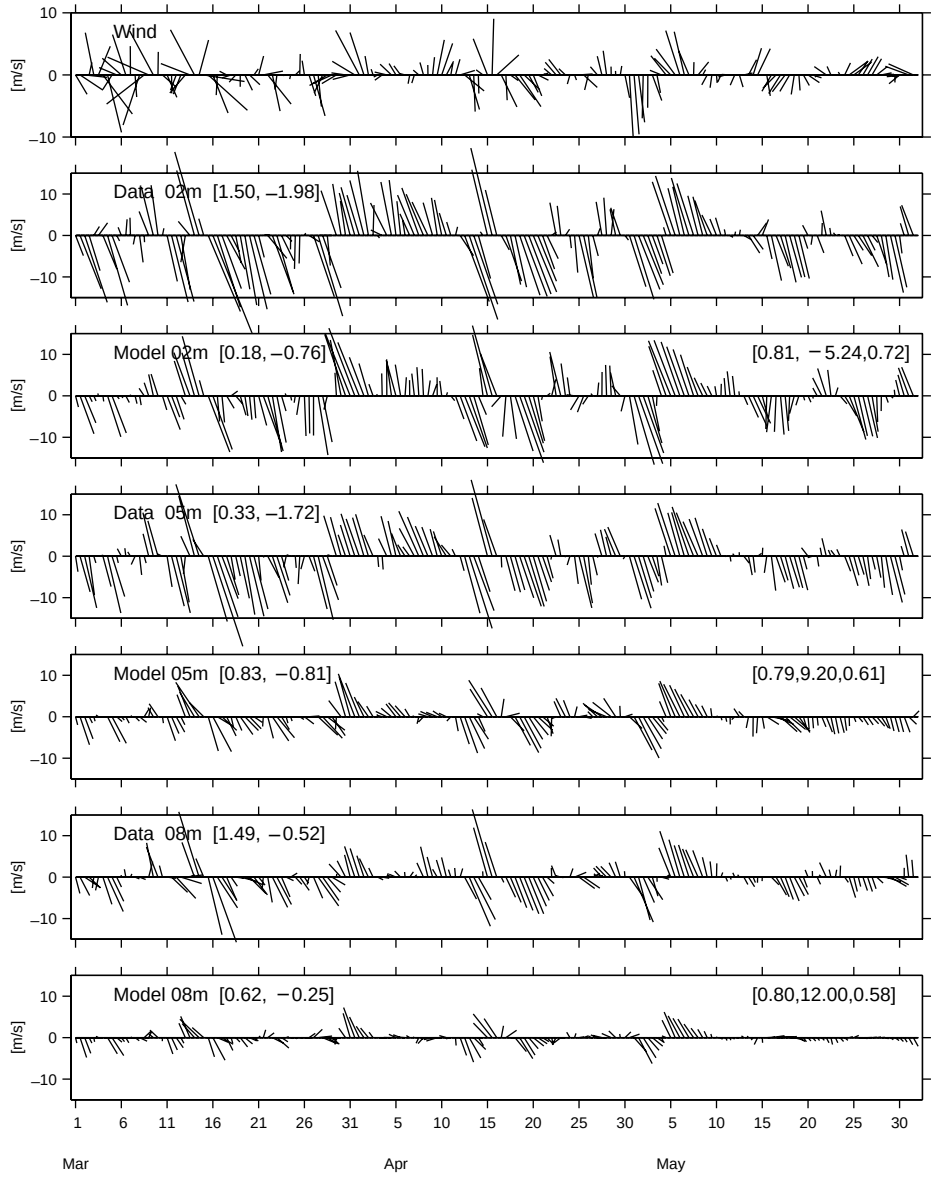

Fig. 5. Comparisons between modeled and observed currents at the 10 m isobath (mooring EC5) sampled at depths of 2, 5 and 8 m, along with the NCEP wind velocity sampled at station A. Quantitative comparisons are as in Fig. 3.

ellipses at all of the mooring locations. The mean vectors compare reasonably well, and while the ellipse semi-major axes are off by between 20–50%, the orientations and eccentricities tend to agree. On the basis of these agreements we now use the model to discuss the WFS circulation in spring 1999.

4. Mean circulation

4.1. Flow fields

The seasonal mean circulation, obtained by averaging the model flow fields from March 1 to May 31, is presented in Fig 7. Three-dimensional

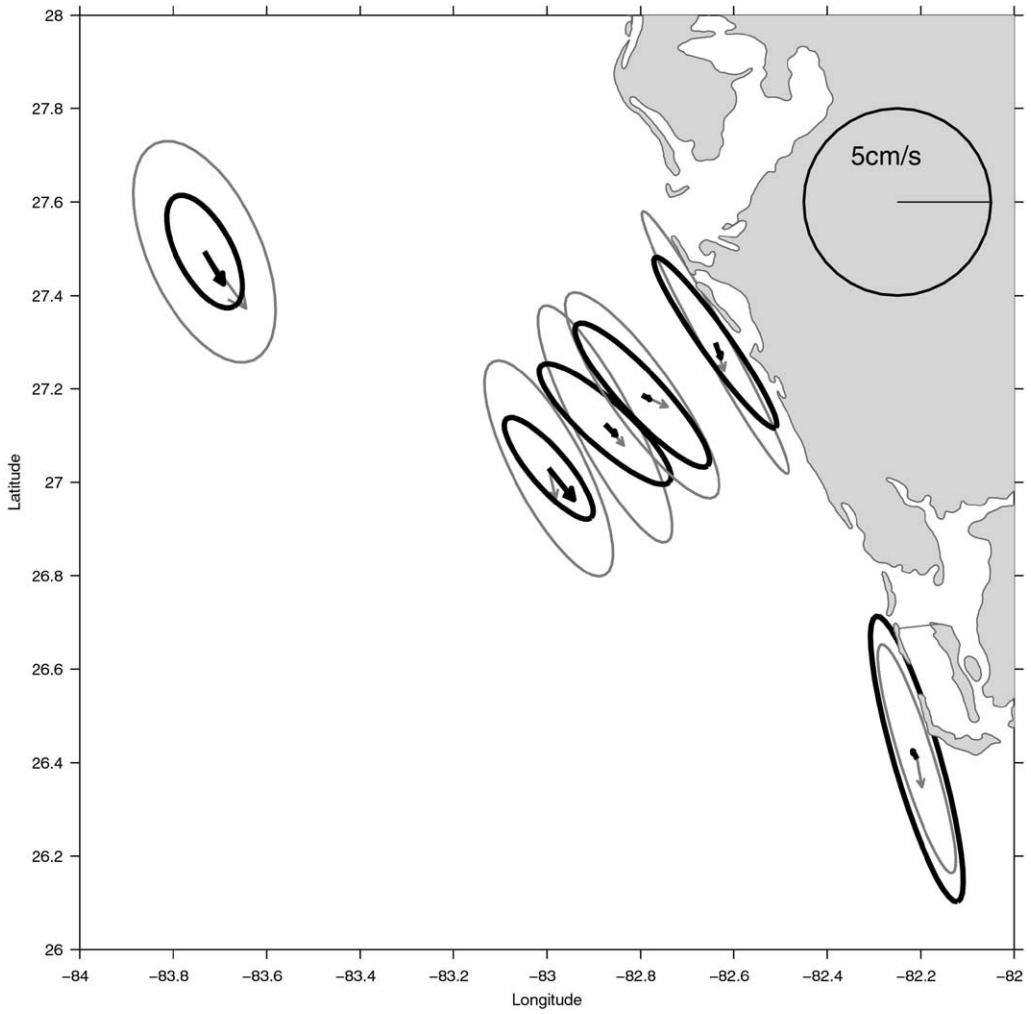

Fig. 6. Comparisons between modeled (bold) and observed (thin) seasonal mean velocity vectors and hodograph ellipses at mid-depth for all six mooring locations on the WFS between the 50 and 10 m isobaths.

flow features arise because of the WFS geometry that includes partial blocking by the Florida Keys, the coastline changes of the Big Bend, and the intrusion of Desoto Canyon. These features are depicted in horizontal velocity field maps given for sigma layers 2 (near-surface), 10 (mid-level), 20 (near-bottom), and for the depth-average.

The mid-level and depth-averaged fields are similar (and with the same scale), and they show the general nature of the 1999 spring season currents. A jet exists with axis situated between the mid-shelf and the shelf break. This jet originates along the northern coast east of the Mississippi River, and it flows along the relatively narrow Florida Panhandle shelf as a closely confined coastal feature. The coastal jet bifurcates at Cape San Blas into a mid-shelf part that heads along-isobath toward the southeast and a coastal part that hugs the Big Bend coastline. The mid-shelf part is consistent with the spring season southeastward current described by Weisberg et al. (1996). This mid-shelf current again bifurcates upon approaching the Florida Keys with a portion turning toward Florida Bay and another portion

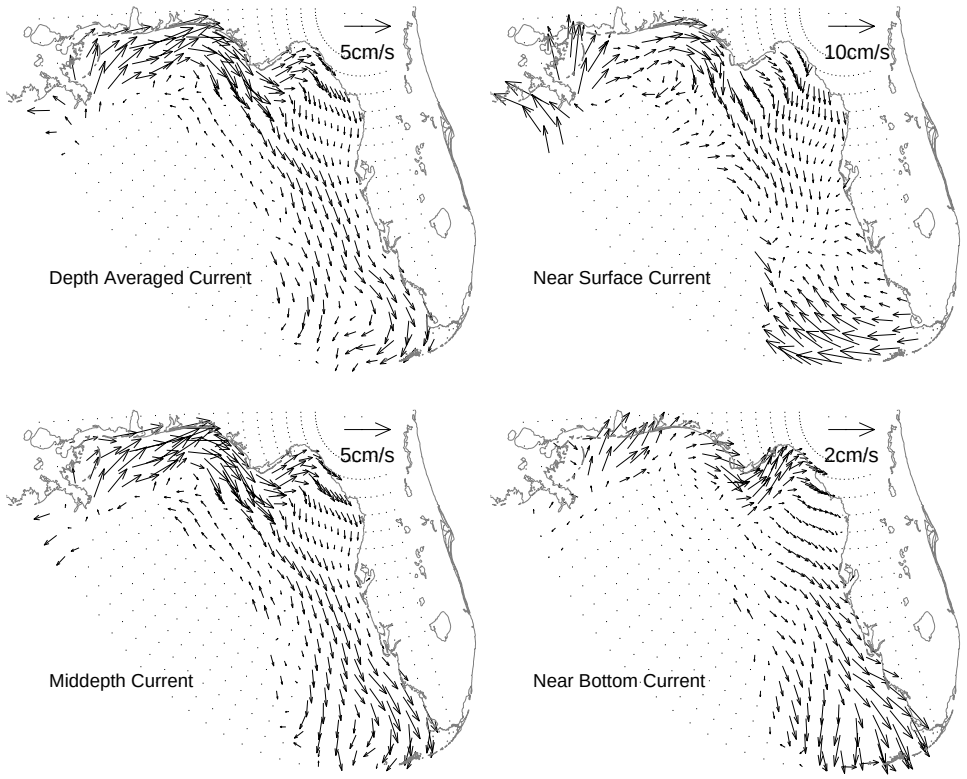

Fig. 7. Modeled seasonal mean velocity vectors for the depth averaged and near-surface, mid-water column, and near-bottom sigma levels, $k = 2$, 10, and 20, respectively.

turning farther offshore. Why this occurs and how it affects the Florida Bay/Florida Keys region are evident in the near-bottom and near-surface flow fields (note the scale changes). Near the bottom we see a convergence of vectors on Florida Bay and the Florida Keys. In contrast to this, near the surface we see flow paralleling the Florida Keys. The near-bottom flow upwells, feeding the near-surface flow, and the second bifurcation is due to the recirculation associated with the upwelling. Li and Weisberg (1999a) discussed a similar recirculation due to the Florida Keys for the case of upwelling winds under a constant density setting. From the surface current map we can appreciate why surface drifters originating in the north do not penetrate the southeast portion of the WFS; the so-called 'Forbidden Zone' described by Yang et al. (1999b). We also note that the currents within the Big Bend and those that flow southward near-shore between Cedar Key and Sarasota are much weaker than the currents at mid-shelf. As will be shown in the next section, this is a consequence of a surface heat flux-induced cyclonic circulation that adds destructively (constructively) to the wind driven flow near-shore (offshore).

Three-dimensionality in the flow field is further evident in the vertical component of velocity shown for near-bottom, middle, and near-surface sigma levels in Fig. 8. Upwelling is prominent north of the Florida Keys with a maximum near the Dry Tortugas, as is often evident in satellite SST imagery (e.g., Weisberg et al., 2000). Upwelling is also prominent west of DeSoto Canyon, around Cape San Blas, and along the west Florida coastline. Other regions show downwelling. This vertical circulation is a function of both the bottom boundary layer and the interior. The

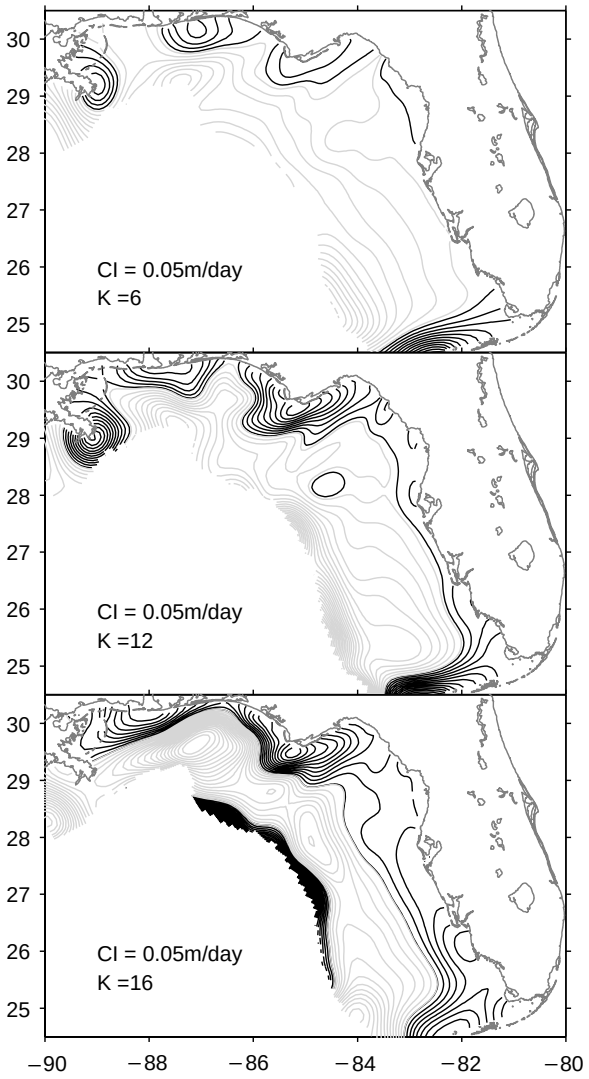

Fig. 8. Modeled seasonal mean vertical velocity component fields (converted to the z-plane) sampled at the near-surface, mid-water column, and near-bottom sigma layers, $k = 6$, 12, and 16, respectively. Bold lines indicate upwelling. Thin lines indicate downwelling.

near bottom w can be reconciled based on the near bottom horizontal velocity field (Fig. 7) and the bottom kinematic boundary condition. Mid-water column divergence then accounts for the transition of w from its near-bottom to near-surface values. Upwelling occurs along the entire near-shore domain near the bottom, whereas upwelling is more localized near the surface.

4.2. Temperature and salinity field

The modeled surface temperature and salinity fields sampled at the end of the model run on May 31 are presented in Fig. 9. Since the initial model temperature and salinity fields are horizontally uniform, this figure shows the combined effects of the momentum and buoyancy fluxes in changing the surface temperature and salinity. The two principal features are the mid-shelf cold tongue that extends southeastward from Cape San Blas and the low salinity tongue that also extends southeastward, but displaced seaward of the cold tongue. Both of these features occur annually on the WFS. The cold tongue is imposed to some extent through the surface heat flux relaxation, whereas the low salinity tongue is a fully prognostic result of the model.

The low salinity tongue derives as a river plume, accumulating fresh water primarily from the

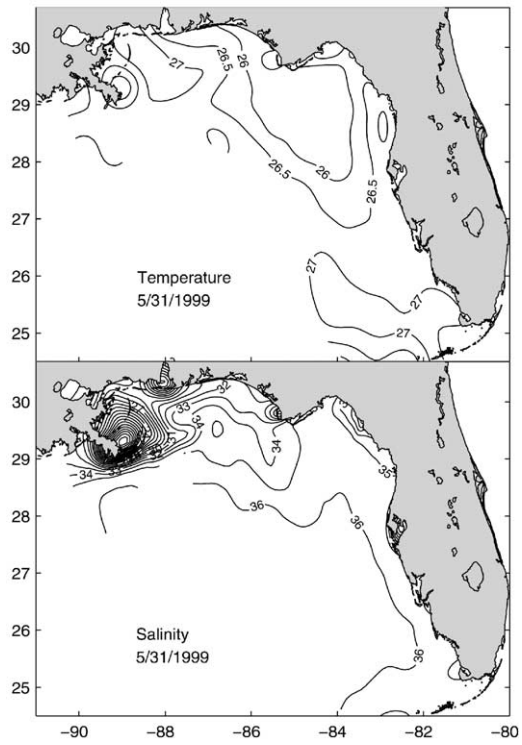

Fig. 9. Sea surface temperature and sea surface salinity fields at the end of spring 1999 model simulation (May 31, 1999).

Mississippi River with additions from the Mobile and Apalachicola Rivers. Modulated interannually, the low salinity tongue extends southward each year, and in some years (1993, for instance—see Dowgiallo et al., 1995) it can be traced around the Florida peninsular to the Carolinas. Using Coastal Zone Color Scanner data between 1979 and 1986, Gilbes et al. (1996) reported a spring chlorophyll plume at mid-shelf (termed the 'Green River') that also extends southeast from Cape San Blas. Their explanations for the plume included: (i) nutrient fluxes from the Apalachicola River; (ii) nutrient fluxes from the Mississippi and Mobile Rivers; (iii) seasonal changes in steric height between the shelf and deeper Gulf of Mexico; and (iv) circulation of water from the Loop Current. Our results help to clarify these speculations. Consistent with Weisberg et al. (1996) the 'Green River' is associated with both the cold tongue and the low salinity tongue. The low salinity tongue, at least in 1999, appears to originate at the Mississippi River. It is advected eastward, on average, by the spring coastal jet and then southeastward where the jet bifurcates at Cape San Blas. This bifurcation, in part, is related baroclinically to the cold tongue; hence the offset between the low salinity and cold tongues. Since the Loop Current is not included in our model, and since it did not extend to the northeast Gulf of Mexico in spring 1999, we can rule out the Loop Current as a primary conveyance of these salinity and temperature features. What remains unclear is the relative importance of land-derived versus upwelling-derived nutrients in fueling the chlorophyll plume. Aggregation of nutrients and phytoplankton by the frontal regions of the cold tongue/low salinity tongue complex can nevertheless account for the 'Green River'.

To explore the roles of momentum and heat flux in the formation of these surface temperature and salinity features we ran a model twin experiment forced by NCEP winds only. Fig. 10 shows the seasonal mean circulation with wind forcing only for comparison with Fig. 7 with both wind and heat flux forcing. Differences occur in all fields. The most obvious is the location of the jet, as seen in either the depth-averaged or the middle level fields. With wind forcing only the jet has a stronger coastal expression over the entire WFS, as contrasted with a stronger mid-shelf jet under wind and heat flux forcing. Baroclinicity explains the difference. With wind and heat flux forcing a dynamical feedback occurs with the cold tongue causing a cyclonic baroclinic circulation that adds constructively (destructively) with the wind forced circulation at mid-shelf (near-shore). A baroclinic circulation also arises without heat flux, but this adds constructively with the wind forced circulation near-shore. This latter effect for wind forcing only is seen in the surface temperature field of Fig. 11. Surface temperature is colder everywhere since the ocean circulation merely rearranges it. By virtue of mean upwelling the near-shore region is colder than the offshore region which causes a southward baroclinic circulation that adds constructively with the southward wind-driven circulation.

Given the importance of surface heat flux on the seasonal circulation it is instructive to see how the baroclinic contribution evolves. This is shown in Fig. 12 for the March, April, and May monthly mean, depth-averaged flows relative to the seasonal mean. March shows an anticyclonic circulation with southeastward flow near-shore. During April, once the effects of positive heat flux set in, we see the formation of the mid-shelf jet and a cessation or reversal of the near-shore flow. This further develops into a strong mid-shelf/shelf-break current in May as the cyclonic baroclinic flow becomes fully developed. This is consistent with the Weisberg et al. (1996) hypothesis on the origin of the springtime southeastward current.

Temperature cross sections at various positions along the WFS provide further information on the cold tongue evolution. These are shown for wind and heat flux forcing and for wind forcing only on March 15, April 15 and May 15, in Figs. 13–15, respectively, at four transects offshore of DeSoto Canyon, Cape San Blas, the Big Bend, and Sarasota. Since the heat flux is initially out of the ocean the March 15 transects, with or without heat flux, are similar at depth. They differ on the shelf where surface cooling, coupled with efficient convective mixing, produces typical wintertime horizontal stratification. By April 15, with a reversal in the sign of the heat flux, the two cases

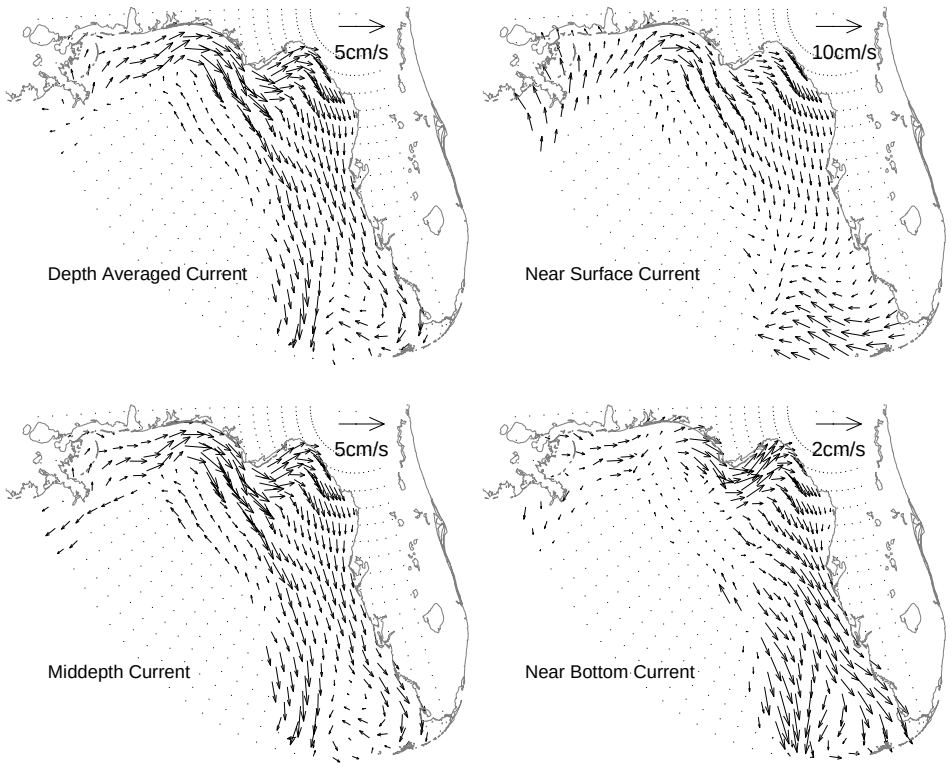

Fig. 10. Modeled seasonal mean velocity vectors for the depth averaged and near-surface, mid-water column, and near-bottom sigma levels, $k = 2$, 10, and 20, respectively, from the model twin experiment forced with wind stress only.

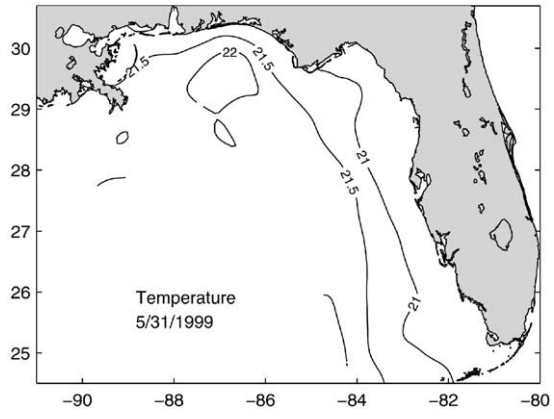

Fig. 11. Sea surface temperature at the end of spring 1999 simulation (May 31, 1999) for the model twin experiment forced by wind stress only.

depart everywhere. The Big Bend transect shows a dome of cold water at mid-shelf in the heat flux case. This originates primarily by the burial (by water being heated from above) of the cold water previously formed in the Big Bend. Water is warmer in the shallows near-shore for the same reason that they were colder in the previous season (a similar heat flux over a shallower layer will result in a larger internal energy change per unit area). There are also secondary contributions from upwelling at the shelf break. Here, the shelf-break upwelling is from the Big Bend as opposed to the DeSoto Canyon, and this is in part a consequence of bottom topography. The shelf break in the Big Bend occurs about 20 m deeper than in the DeSoto Canyon. Hence, less upwelling is required for water to rise onto the shelf in the Big Bend than in the DeSoto Canyon. This finding is clear in

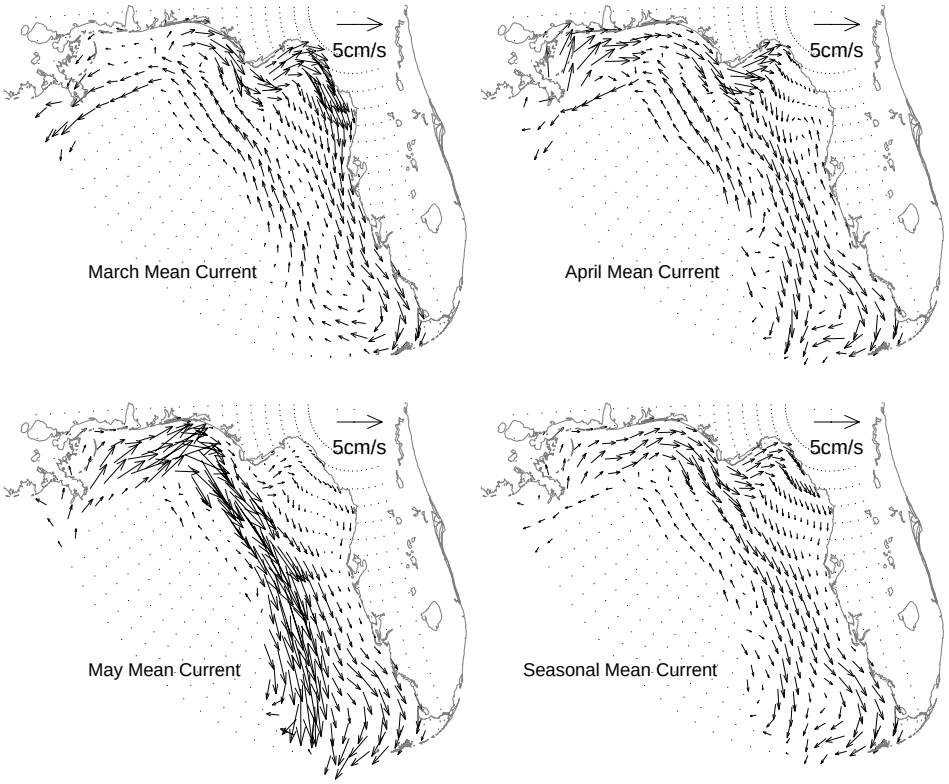

Fig. 12. Evolution of the monthly mean, depth averaged velocity vectors for March, April, and May relative to the spring 1999 seasonal mean.

continuous animations where we also see that the advective time scale between the DeSoto Canyon and the Big Bend is longer than the synoptic weather time scale. For spring 1999, at least, we do not see a direct connection between the DeSoto Canyon and Big Bend regions as would be evidenced by continuous isotherms. Note that while 21°C waters occur on the shelf offshore of both the DeSoto Canyon and Big Bend regions these waters are not seen on the shelf at the intervening Cape San Blas cross section. Local upwelling in the Big Bend region (due to a relatively deep shelf break) is therefore important, and it may help to explain the relatively high productivity of the Florida Middle Grounds. A similar subsurface cold-water core is seen farther south off Sarasota and for the same reasons. It is smaller in magnitude because of differential cooling and heating from north to south, i.e., when the heat flux reversed from cooling to warming the temperatures off Sarasota were already warmer than those in the Big Bend. Dynamically, the doming of cold water at mid-shelf (and hence the cold tongue) induces the cyclonic baroclinic circulation. This is further facilitated by the no heat flux bottom boundary condition that bends the isotherms perpendicular to the bottom. These combined effects of differential heating (near-shore to offshore by bottom slope and southward to northward by solar declination) and dynamical feedbacks (baroclinic pressure gradients associated with the temperature gradients) conspire to cause the spring season temperature transition from well mixed to stratified with a cold tongue at mid-shelf.

The May 15 transects show the continued evolution of these processes. By now the mid-shelf

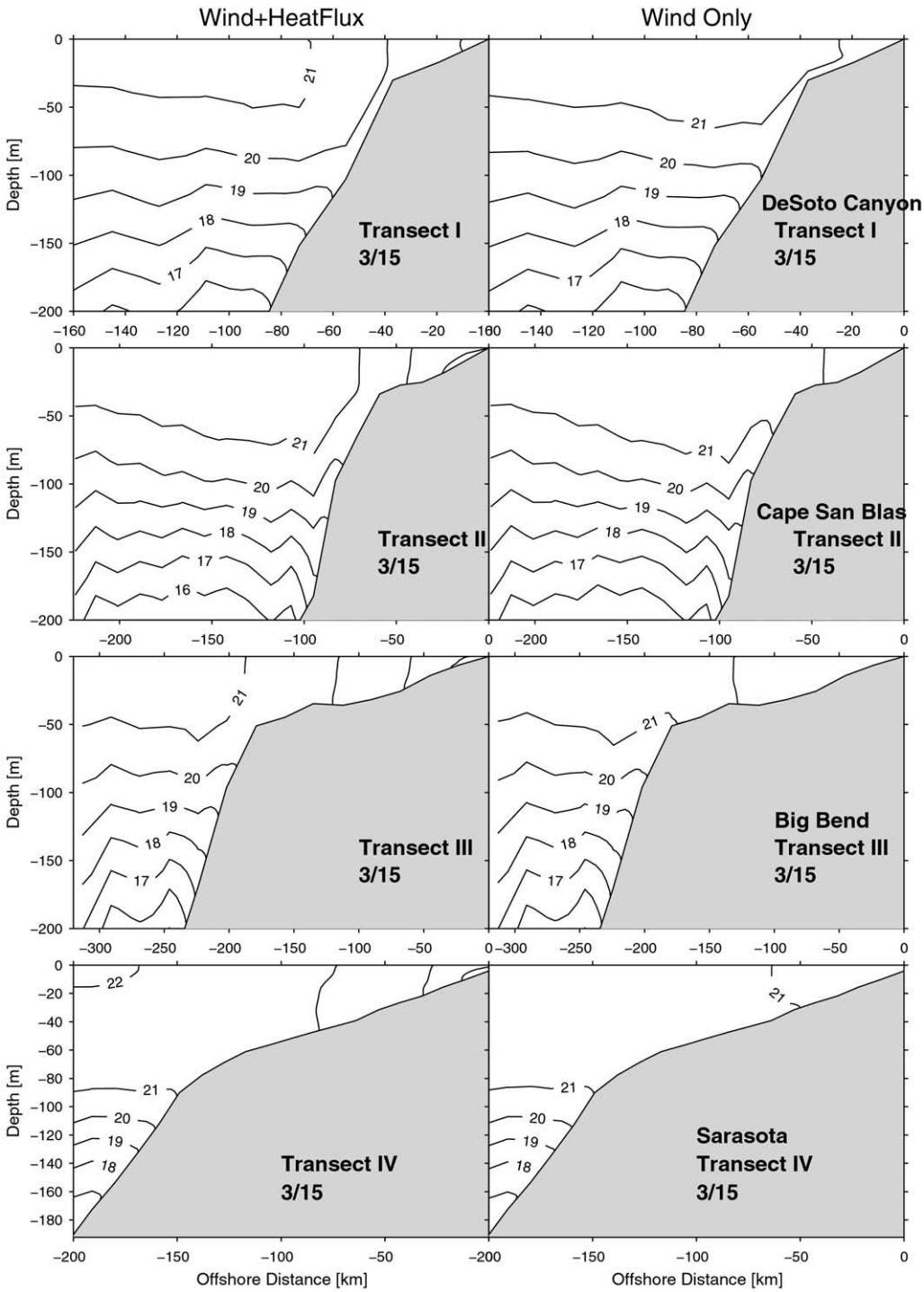

Fig. 13. Modeled temperature sections sampled on March 15 across transects originating at DeSoto Canyon, Cape San Blas, Florida Big Bend, and Sarasota. The contour interval is 1°C.

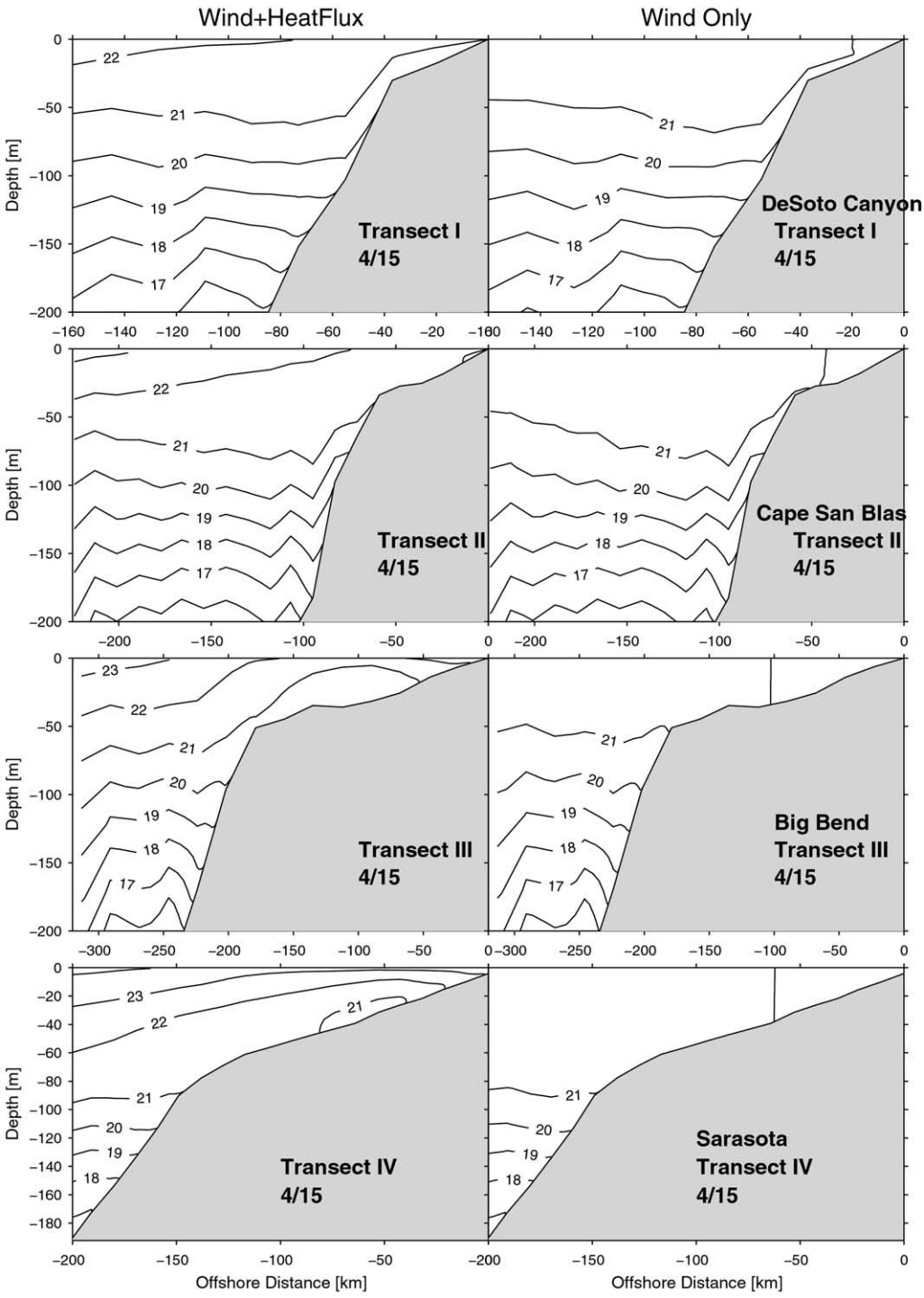

Fig. 14. Same as Fig. 13 except sampled on April 15.

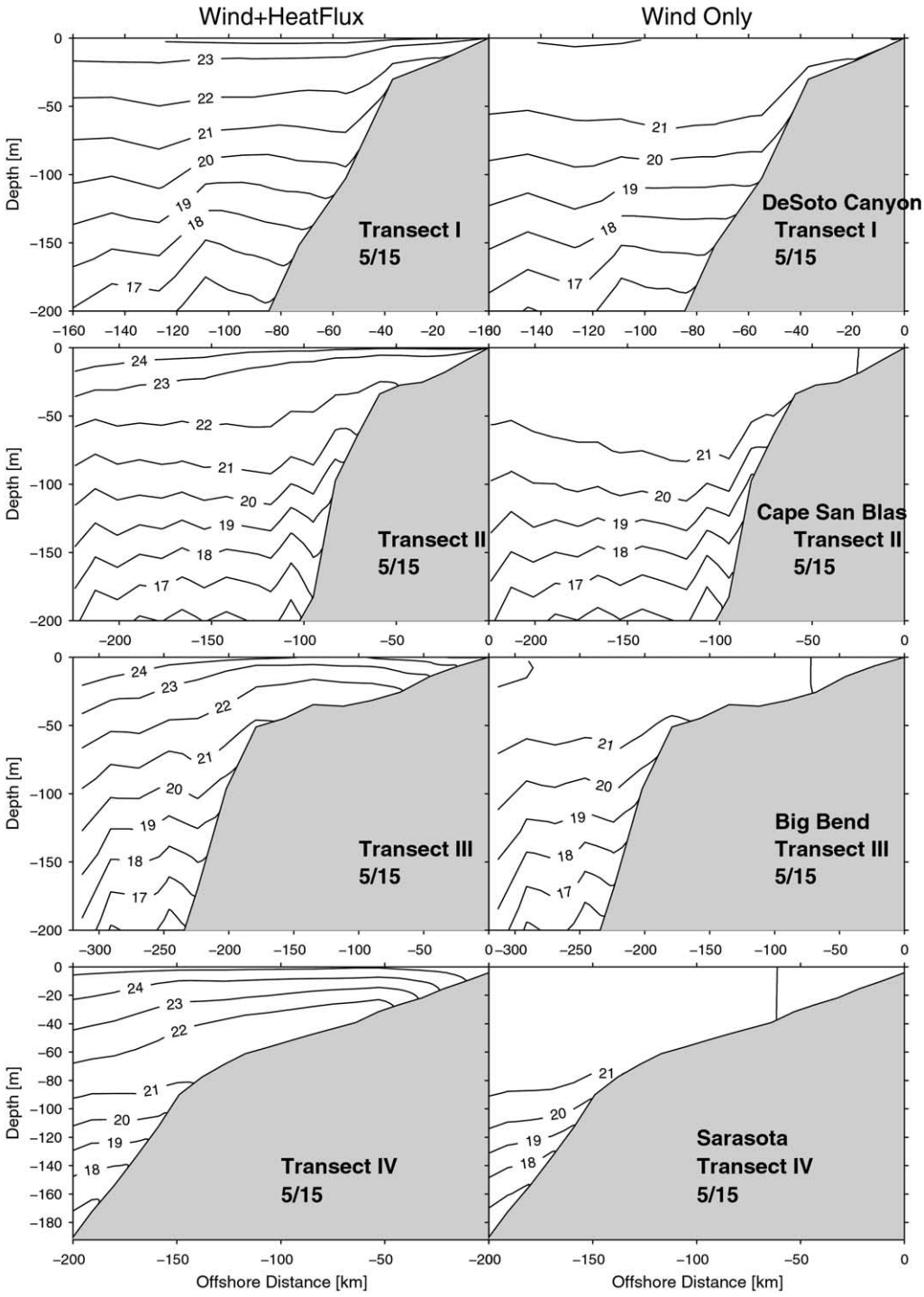

Fig. 15. Same as Fig. 13 except sampled on May 15.

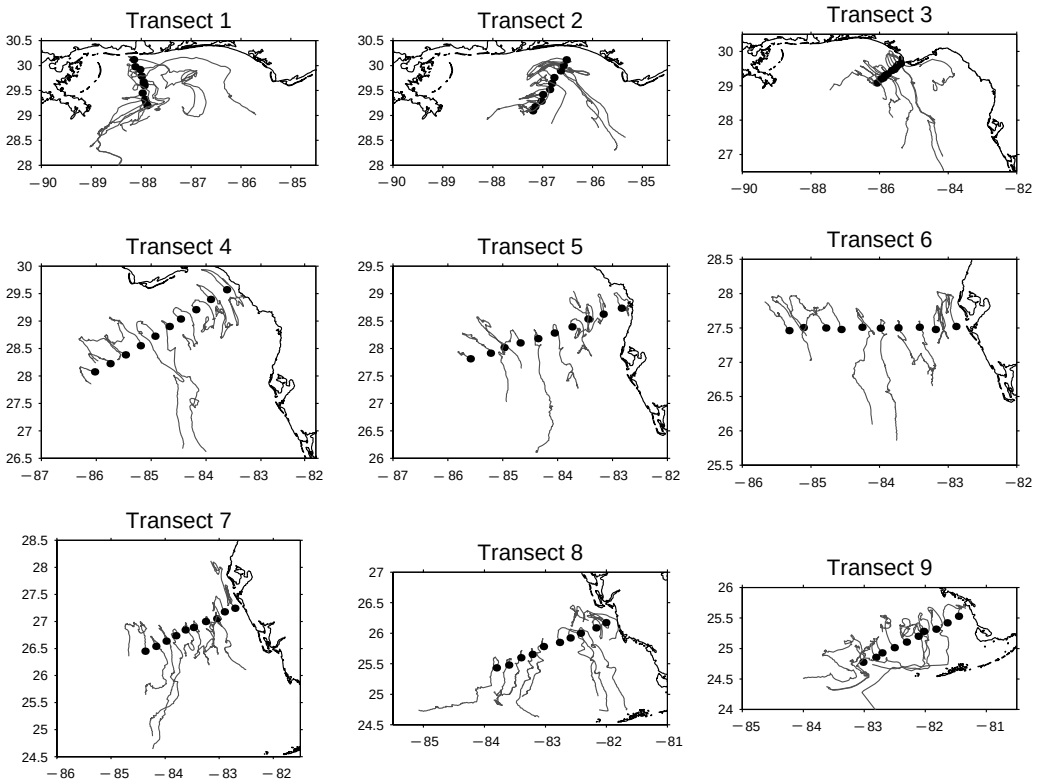

Fig. 16. Modeled near-surface Lagrangian drifter trajectories for the period April 1, 1999–May 31, 1999. Drifters were started along nine different transects with initial positions given by solid dots.

isotherm doming has relaxed due to continued heating and so has the mid-shelf circulation due to decreased winds and baroclinicity. The location of the jet is now farther offshore at the shelf break, and the modeled temperature agrees with observed ECOHAB Program hydrography.

4.3. Lagrangian drifters

Model-simulated Lagrangian drifter tracks provide additional information on the evolution of the cold and low salinity tongues and the regions for possible communication between the deep ocean and the shelf. Dynamically passive particles released in the model on April 1st are tracked through May 31st. These are shown in Figs. 16 and 17 for particles originating either near the surface or the bottom, respectively. Most evident for the particles released near the surface is advection by the mid-shelf jet and the bifurcations at Cape San Blas and north of the Florida Keys. The particle trajectories agree with the Eulerian maps previously shown and with the cold and low salinity tongue features. With the exception of those in the mid-shelf jet the particle displacements are not very large. The near-surface drifters also show a propensity to flow either along-isobath or offshore. The near-bottom released drifters show subtle, but important differences, particularly in the Florida Big Bend/Middle Ground region. There we see onshore flow between the shelf break and the mid-shelf. This is consistent with the changes in hydrography discussed in the previous section, supporting our speculation that the Big Bend may be an important region for deep ocean/shelf interactions.

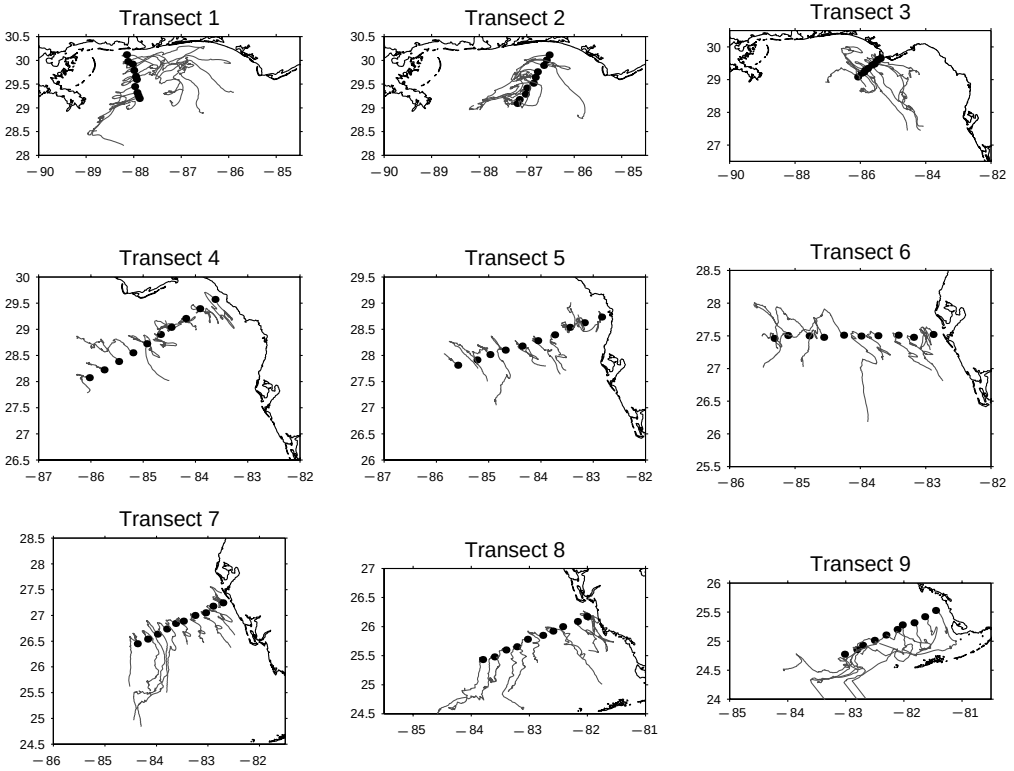

Fig. 17. Same as Fig. 16 except for near-bottom Lagrangian drifter trajectories.

5. Temperature budget

5.1. The temperature equation

To analyze the temperature budget, the temperature equation is recast from its modeled flux divergence, *sigma level* form to an advective, *z-level* form. Thus, we diagnose

$$\underset{a}{\frac{\partial T}{\partial t}} = \underset{b}{-u\frac{\partial T}{\partial x}} \underset{c}{- v\frac{\partial T}{\partial y}} \underset{d}{- w\frac{\partial T}{\partial Z}} + \underset{vf}{\frac{\partial}{\partial z}\left(K_H \frac{\partial T}{\partial z}\right)} + \underset{hf_y}{\frac{\partial}{\partial x}\left(A_H \frac{\partial T}{\partial x}\right)} + \underset{hf_x}{\frac{\partial}{\partial y}\left(A_H \frac{\partial T}{\partial y}\right)} \quad (3)$$

which equates the local rate of change of temperature (a) to a combination of the flow field advective rate of change ($b + c + d$), and the rates of change by vertical diffusion (vf), and horizontal diffusion ($hf_x + hf_y$). The temperature balance is explored using: (i) time series of vertical averages, (ii) time series of vertical profiles at four different locations, and (iii) term by term spatial maps of the sea surface temperature rates of change.

The four analysis locations (see Fig. 1) are chosen with respect to the cold tongue and the upwelling region north of the Florida Keys. Point A is on the 50 m isobath at the seaward side of the Big Bend shelf subsurface cold dome. Point B is on the 40 m isobath west of Tampa Bay where the cold tongue begins to taper off. Point C is on the 15 m isobath offshore of Sarasota on the inshore side of the cold tongue. Point D is north of the Florida Keys. A term-by-term analysis of (3) quantifies the contributions by each physical process in changing the temperature.

5.2. Depth-averaged balances

A depth-averaged temperature equation is obtained by vertically integrating Eq. (3). Since horizontal temperature diffusion is generally at least an order of magnitude less than the other terms, the depth-averaged diffusion term is essentially the depth-averaged vertical diffusion, $Q/(\rho C_P H)$, where Q is the net surface heat flux, ρ and C_P are the seawater density and specific heat, and H is the water depth. The temperature variations depend on both ocean advection and diffusion. With a two-dimensional model, Morey (1999) proposed that temperature, in a depth-averaged sense, could be well represented without advection, i.e.,

$$\frac{\mathrm{d}T}{\mathrm{d}t} = \frac{\partial T}{\partial t} = \frac{Q(t)}{\rho c_P H}. \tag{4}$$

The validity of this assertion for various locations on the WFS can be evaluated by a fully three-dimensional analysis.

Time series of the depth-averaged ocean advection and diffusion terms and their sum for locations A–D are shown in Figs. 18a–d, respectively. While not shown in these figures, we note that the sum of these two terms is nearly exactly equal to the negative of the local rate of temperature change, which is essentially a check on our budget analysis. At station A, the depth-averaged rates of change are relatively small, and a clear distinction exists between the balances occurring on seasonal and synoptic time scales. The seasonal change (as given by the three-month mean values) is primarily by surface heat flux, whereas the synoptic variability (as given by the standard deviations) is primarily by ocean advection. Although a relatively small contribution to the seasonal change, the ocean advection does provide a cooling influence that offsets the surface heating by about 4% at this location. Thus, of the total change in vertically averaged temperature (1.66°C), the contributions by ocean circulation and surface heat flux are a cooling of −0.07°C and a warming of 1.73°C, respectively. In contrast with the seasonal change, for synoptic scale variability we see that the ocean circulation is twice as effective as the surface heat flux in changing the vertically averaged temperature at station A.

Somewhat different results are found at station B. While surface heat flux and ocean circulation again control the seasonal and synoptic scale variability, respectively, the relative magnitudes and the signs change. Of the total change in vertically averaged temperature (3.05°C), both the ocean circulation and the surface heat flux at the southern terminus of the cold tongue contribute to warming at 0.68°C and 2.37°C, respectively. The ocean circulation also plays a proportionately larger role in the synoptic scale variability at station B than at station A.

The relative importance of the ocean circulation versus surface heat flux continues to change approaching shallower water. At the 15 m isobath, station C, of the total change in vertically averaged temperature (4.76°C), the contributions by ocean circulation and surface heat flux are cooling of −1.24°C and a warming of 6.00°C, respectively. The shallower the water, the larger the total spring transition change. However, the role of the ocean circulation in this change varies in both magnitude and sign with location. For instance, at station D in the upwelling region north of the Florida Keys, the ocean circulation provides a cooling influence of 2.79°C that partially offsets the surface heat flux warming influence of 8.11°C. Without the upwelling influence by ocean circulation the water temperature north of the Florida Keys would be much warmer. Along with these increased effects by the ocean circulation on the seasonal mean temperature change, the magnitude of the controlling ocean circulation effect on the synoptic scale variability also increases with decreasing water depth. The temperature budget on all time scales is a complex one requiring a fully three-dimensional description.

5.3. Vertical profiles of the term by term balances

The temperature budget three-dimensionality is further explored through time series of the depth profiles of the individual terms that comprise the temperature balance at these four stations (Figs. 19–22). In each of these figures the left-hand panels show the horizontal and vertical

components of the ocean advection and their sum, and the right-hand panels show the diffusion, the diffusion plus the advection (which is nearly exactly equal to the negative of the local rate of change of temperature), and the temperature. With the exception of the initial portion of the record when the surface heat flux is out of the ocean and convective mixing is evident, the immediate impact of the surface heat flux is primarily in the near-surface region (Fig. 19).

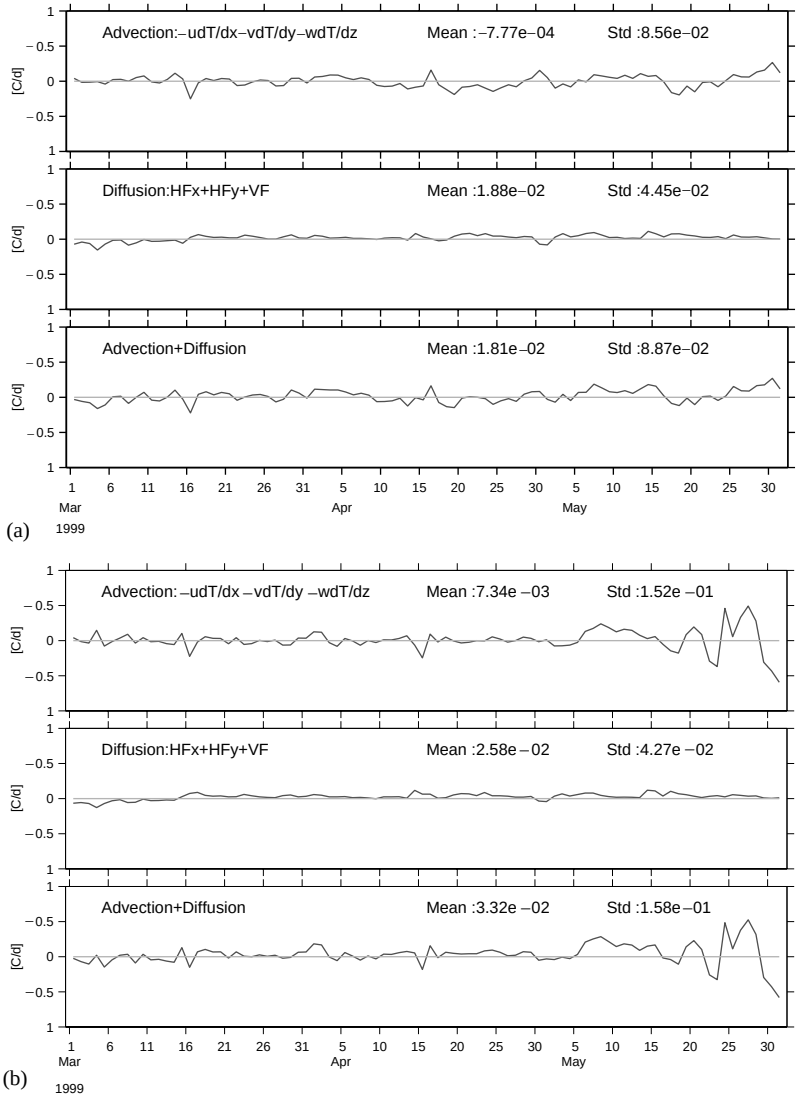

Fig. 18. (a) The relative contributions to the depth-averaged temperature balance by ocean circulation and diffusion at station A. Three time series are shown: the advection, the diffusion, and their sum (which equals the local rate of change of depth-averaged temperatuere). Accompanying each time series are their seasonal means and standard deviations in units of $^{\circ}$C day^{-1} as measures of the seasonal and synoptic scale variability. (b) Same as Fig. 18a except for station B. (c) Same as Fig. 18a except for station C. (d) Same as Fig. 18a except for station D.

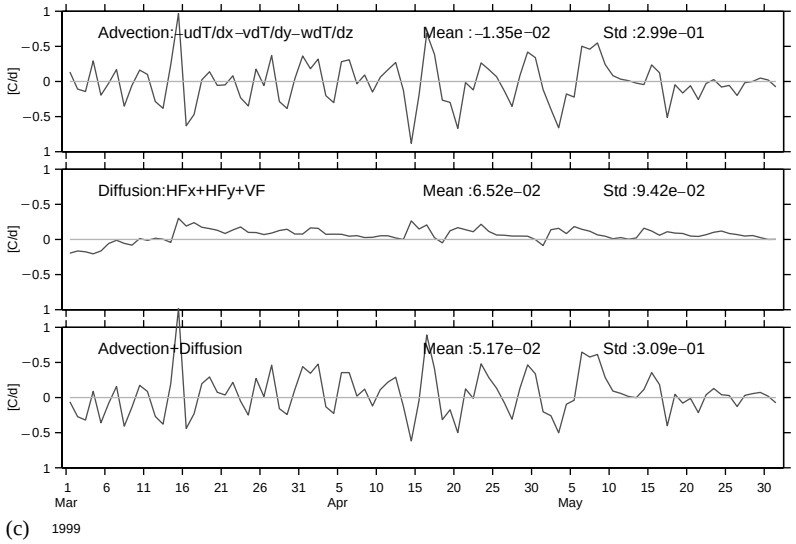

(c)

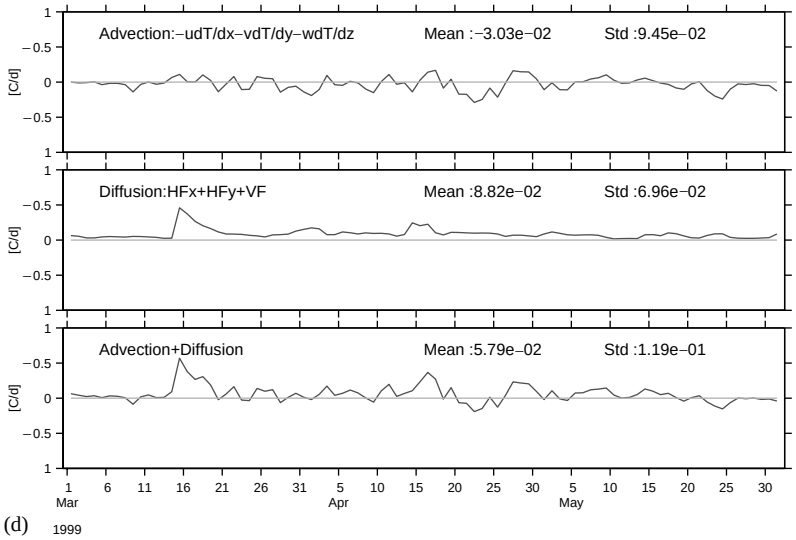

(d)

Fig. 18. (*continued*)

Without convective mixing, it is then only through turbulence mixing, brought about by the ocean circulation dynamics, that the surface heat flux effect accumulates downward to make its contribution to the depth-averaged spring transition. From the vertical distributions of the seasonal means shown to the right of each panel we see that turbulence mixing distributes the surface heat flux over about 20 m depth. Along with its role in turbulence mixing, the direct role of the ocean dynamics through advection on the synoptic scale variability is seen in both horizontal and vertical directions. Omission of any coordinate direction would compromise the model's ability to describe the temperature evolution. For instance, the strong stratification at the end of May at station

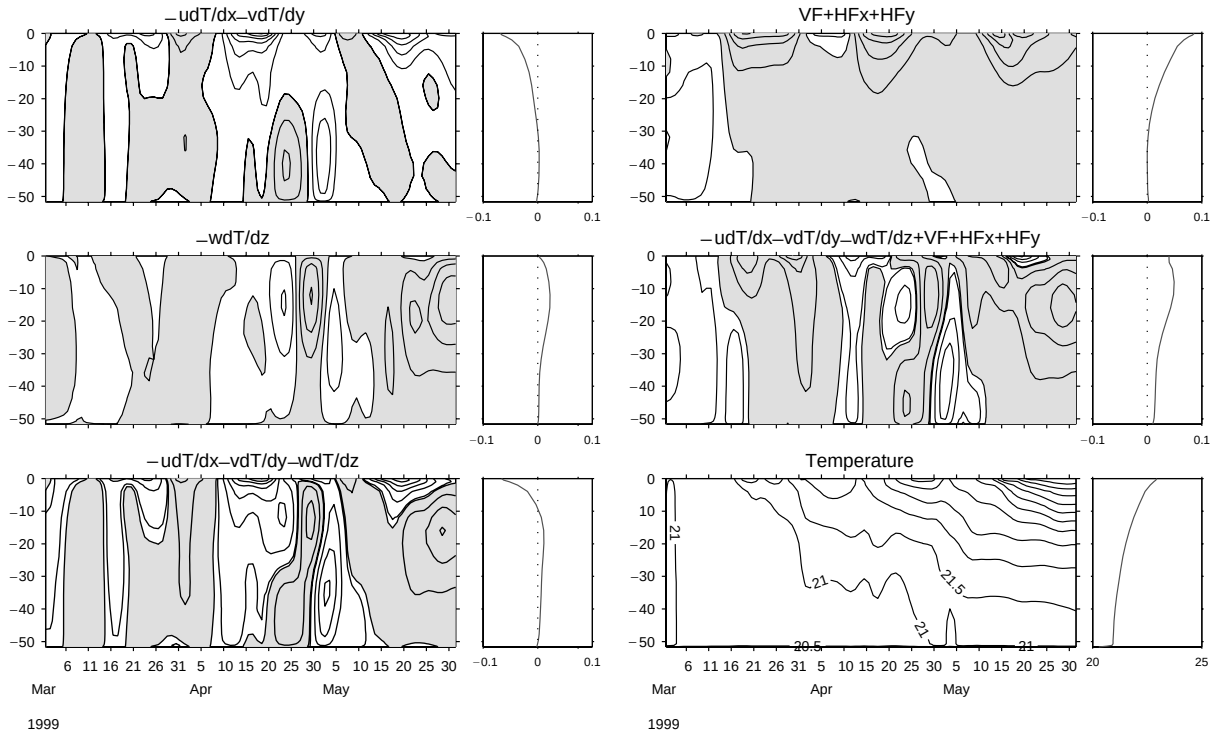

Fig. 19. Time series of the depth profiles of the individual terms that comprise the temperature balance at station A. The left-hand panels show the horizontal and vertical components of the ocean advection and their sum, and the right-hand panels show the diffusion, the diffusion plus the advection, and the temperature. To the right of each panel is the seasonal mean profile. The contour interval for each of the budget terms is 0.05°C day^{-1}, and the contour interval for temperature is 0.5°C. Shading indicates warming and clear indicates cooling.

A is due largely to the combined effects of horizontal and vertical advection. Similar conclusions follow from station B (Fig. 20). Station C (Fig. 21), in shallow water, shows the additional effect of turbulence mixing in the bottom Ekman layer. Here, temperature is elevated near the bottom by ocean circulation-induced mixing. The role of the ocean circulation in promoting mixing is seen in the covariability between the advection and diffusion terms. These interactions are even more evident at station D (Fig. 22) where warming by near-bottom turbulence mixing is required to partially offset the cooling influences by horizontal advection and upwelling. Another interesting feature of the shallow water regions is the tendency for large changes in stratification by the ocean circulation. Two downwelling events culminating in destratification and warming by advection are seen at station C around April 5th and May 10th. Similarly, but in an opposite sense, stratification caused by horizontal advection is seen at this station at the end of May.

5.4. Term-by-term contributions to the seasonal change in SST

The contributions to the seasonal mean rate of change of sea surface temperature (SST) by each of the advection and diffusion terms are discussed with respect to Fig. 23. The left panels show the advection terms and their sum, and the right panels show the horizontal and vertical diffusion terms, and the sum of all terms. Of particular interest here is the spatial distribu-

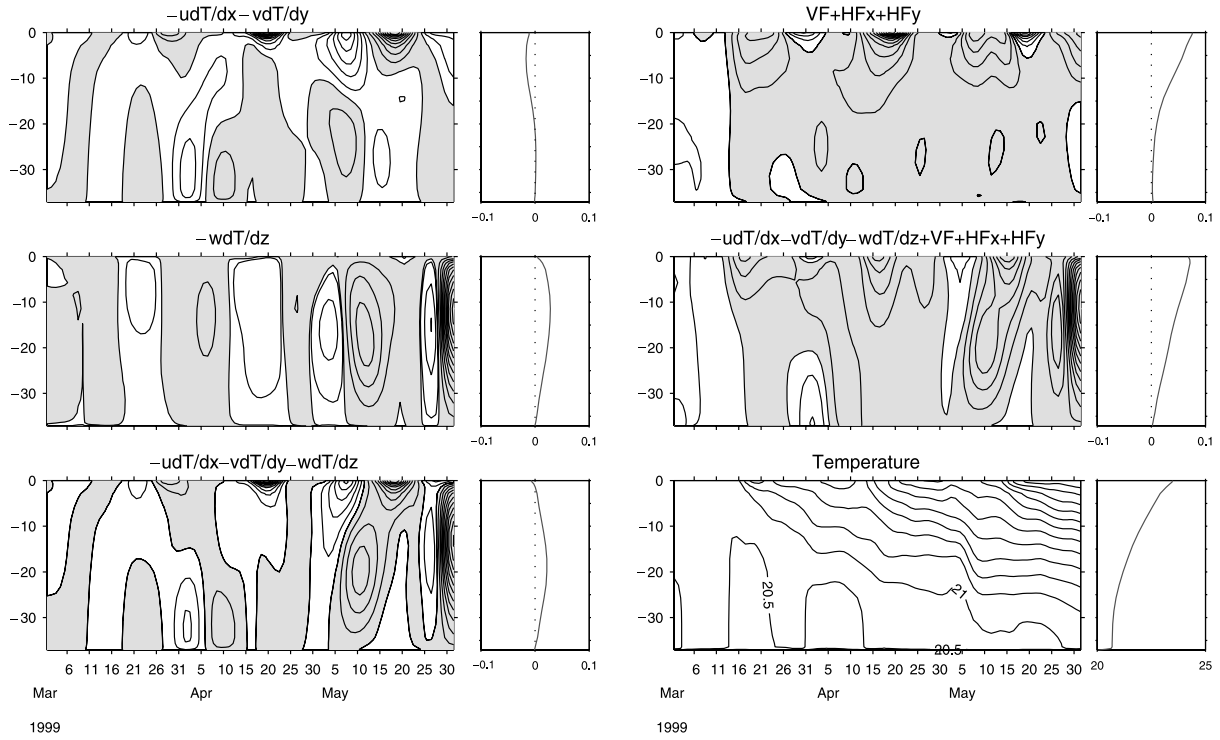

Fig. 20. Same as Fig. 19 except for station B.

tion of the processes controlling SST over the model domain. Horizontal diffusion is minimal everywhere except for north of the Florida Keys where it is still the smallest of the terms. Vertical diffusion controlled by the surface heat flux, warms everywhere with maximum warming tendencies stretching along mid-shelf from the Big Bend to the Florida Keys. This warming is the seasonal signal associated with spring, which displays the spatial inhomogeneities mentioned earlier. The difference between this map and the local rate of change of SST is the ocean circulation. By advecting relatively cool water southward, advection provides a cooling influence over the WFS with largest values north of the Florida Keys. With regard to total advection, Cape San Blas divides the entire domain into two sections. To the west, and extending along the north Florida coastline to the Mississippi River, advection tends to provide a warming influence, whereas to the east, along the west Florida coastline, advection tends to provide a cooling influence. Without advection, the center of the cold tongue on the WFS would be some 3–5°C warmer.

6. Summary

Mid-latitude continental shelves undergo a spring transition as the net surface heat flux changes from cooling to warming. Using in situ data and a numerical circulation model we investigate the circulation and temperature budget on the WFS, including the northeast Gulf of Mexico shelf from the Mississippi River to the Florida Keys, for the spring transition of 1999. The data consist of sea level from coastal stations, velocity profiles from instruments moored across the shelf between the 50 and 10 m isobaths, and hydrography from ship sur-

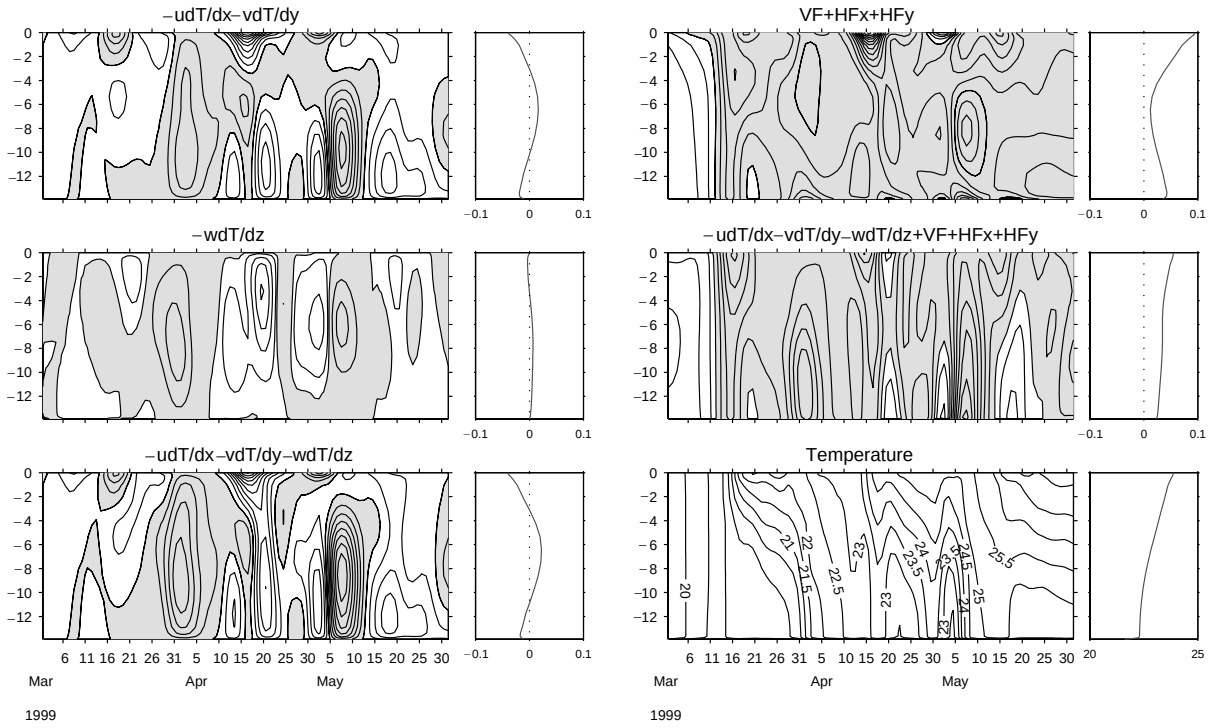

Fig. 21. Same as Fig. 19 except for station C.

veys. The model is a regional adaptation of the primitive equation, POM forced by NCEP reanalysis wind stress and heat flux fields and by river inflows. Based on agreements between the modeled and observed fields we use the model to draw inferences on how the surface momentum and heat fluxes affect the seasonal and synoptic scale variability.

Spring season features of the WFS include a mid-shelf southeastward current, cold and low salinity tongues, and a high chlorophyll plume. We account for the southeastward current in 1999 by the combined responses to local, shelf-wide wind and buoyancy forcing. Wind stress drives a circulation that tends to be strongest near-shore. Heat flux provides a cyclonic contribution that adds constructively (destructively) at mid-shelf (near-shore), thus forming the observed mid-shelf jet. This heat flux-induced baroclinic circulation is related to the spring season cold tongue. By advecting Mississippi (and other) River water it forms the low salinity tongue that is displaced seaward of the cold tongue. Convergence of nutrients and associated phytoplankton growth then accounts for the high chlorophyll concentrations ('Green River') that are co-located with these surface features. These findings support the hypothesis advanced by Weisberg et al. (1996b) on the origin of the southeastward current and cold tongue through differential heating from the coast to offshore (by shoaling topography) and from south to north (by solar declination). Since we arrive at these features with a model experiment that explicitly omits the Gulf of Mexico Loop Current we argue that the Loop Current is not an essential element of these spring transition features.

Through term-by-term analyses of the temperature budget we describe the evolution of WFS temperature in spring. Surface heat flux largely controls the seasonal transition, whereas ocean circulation largely controls the synoptic

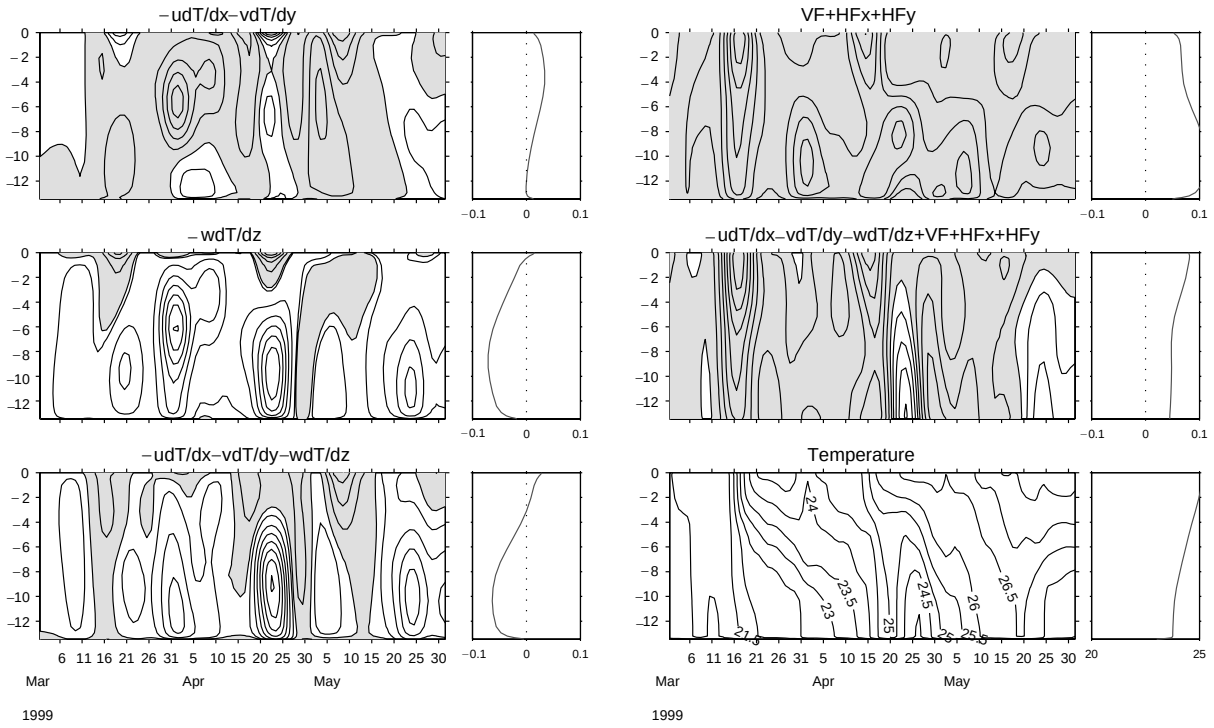

Fig. 22. Same as Fig. 19 except for station D.

scale variability. These two processes are closely linked, however. Since the ocean circulation controls the turbulence mixing, the effects of the ocean circulation are of increasing importance with decreasing water depth. For instance, warming by turbulence mixing near the bottom only occurs when the bottom Ekman layer is well developed by strong currents. Thus, the water column can warm even under upwelling influence if the mixing is large enough. The water column is also found to either stratify or destratify in response to ocean circulation changes. Examples of these effects are shown. While our temperature analyses support the Morey (1999) one dimensional temperature balance argument advanced on the basis of a two-dimensional model, we demonstrate that the temperature balance is more complicated in time and space and requires fully three-dimensional thermodynamics.

Bottom topography and coastline geometry are important in generating regions of convergence and divergence and hence upwelling centers. In particular, we show that the region north of the Florida Keys has strong upwelling in spring and we speculate on the importance of the Florida Big Bend as a region for communication between the deeper Gulf of Mexico and the WFS. The shelf break there is about 20 m deeper than at the DeSoto Canyon thereby requiring less upwelling for deeper waters to broach the shelf. This may be one reason why the Florida Middle Grounds are productive. The northeast Gulf of Mexico shelf from Cape San Blas to the Mississippi River also shows mean upwelling during spring 1999.

Acknowledgements

This work was supported by grants from the Office of Naval Research, grant # N00014-98-1-0158 and the National Oceanic and Atmospheric Administration, grant #NA76RG0463. We also

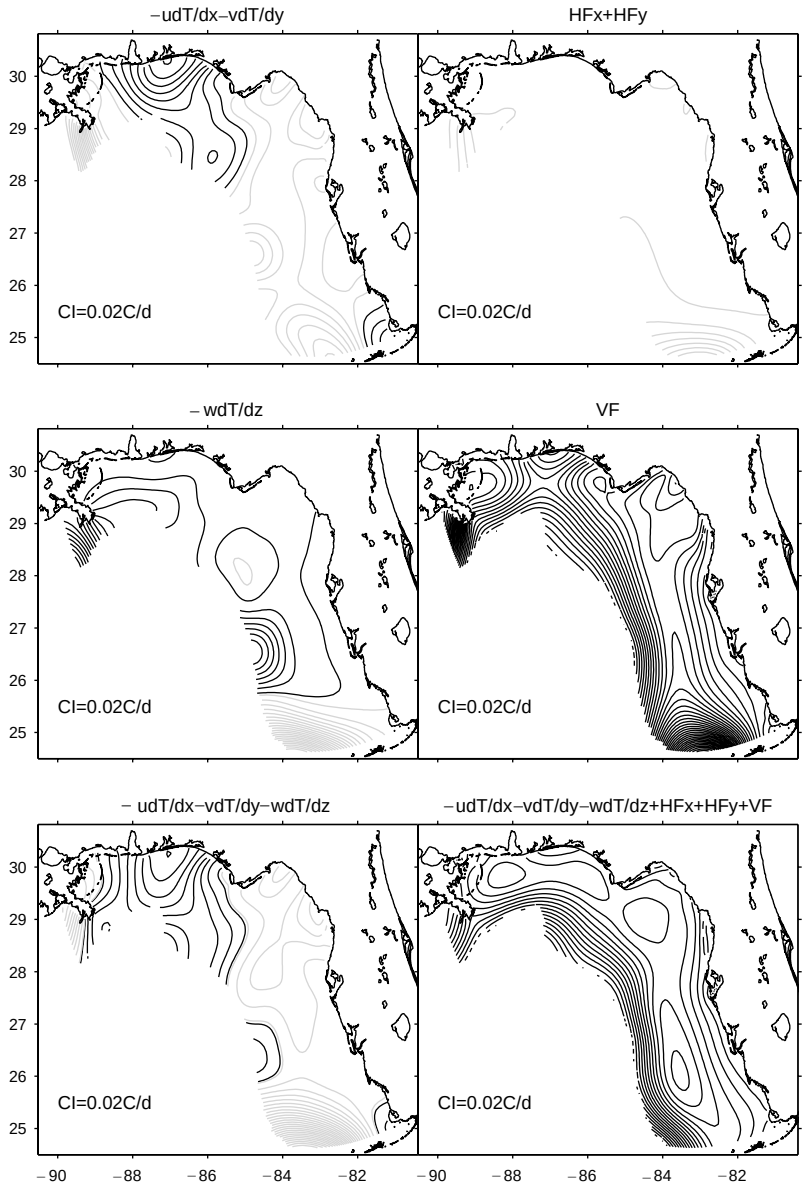

Fig. 23. The contributions made to the seasonal mean rate of change of SST by each of the advection and diffusion terms. The left panels show the advection terms and their sum, and the right panels show the horizontal and vertical diffusion terms, the sum of all terms. The contour interval is 0.02°C day^{-1}. Bold lines indicate warming and thin lines indicate cooling.

benefited from an evolving program with previously support from the United States Geological Survey and the Minerals Management Service. Ocean Circulation Group staff (Messrs. R. Cole, J. Donovan, C. Merz, and P. Smith) contributed to the field work and analyses, as did students W. Hemme and J. Virmani. We thank F. Muller-Karger for providing assistance with the monthly mean SST fields and Z. Li for helpful discussions on the model diagnostics. NCEP re-analysis data

provided by NOAA-CIRES Climate Diagnostics Center, Boulder, CO was obtained from their web site at http://www.cdc.noaa.gov/

References

Blumberg, A.F., Mellor, G.L., 1987. A description of a three-dimensional coastal ocean circulation model. In: Heaps, N. (Ed.), Three-Dimensional Coastal Ocean Models, Vol. 4. AGU, Washington DC, pp. 208–233.

Chapman, D.C., Gawarkiewicz, G., 1993. On the establishment of the seasonal pycnocline in the Middle Atlantic Bight. Journal of the Physical Oceanography 23, 2487–2492.

Chu, P., Edmons, N., Fan, C., 1999. Dynamical mechanisms for the south China sea seasonal circulation and thermohaline varibilities. Journal of the Physical Oceanography 29, 2971–2989.

Clarke, A.J., Brink, K.H., 1985. The response of stratified, frictional flow of shelf and slope waters to fluctuating large-scale, low-frequency wind forcing. Journal of the Physical Oceanography 15, 439–453.

Cooper, C., 1987. A numerical modeling study of low-frequency circulation on the West Florida shelf. Coastal Engineering 11, 29–56.

Cragg, J., Mitchum, G., Sturges, W., 1983. Wind-induced sea-surface slopes on the West Florida shelf. Journal of the Physical Oceanography 13, 2201–2212.

Dowgiallo, M.J. (Ed.), 1995. Coastal Oceanographic Effects of the Summer 1993 Mississippi River Flooding. Special NOAA Report, March 1994, 77pp.

Ezer, T., Mellor, G., 1992. A numerical study of the variability and separation of the Gulf Stream, induced by surface atmopheric forcing and lateral boundary flows. Journal of the Physical Oceanography 22, 660–682.

Galperin, B., Kantha, L.H., Hassid, S., Rosati, A., 1988. A quasi-equilibrium turbulent energy model for geophysical flows. Journal of Atmospheric Sciences 45, 55–62.

Gaul, R.D., 1967. Circulation over the continental margin of the northeast Gulf of Mexico. Ph.D. Dissertation, Department of Oceanography, Texas A&M University, College Station, 156pp.

Gilbes, F., Thomas, C., Walsh, J.J., Muller-Karger, F.E., 1996. An episodic chlorophyll plume on the West Florida shelf. Continental Shelf Research 16, 1201–1224.

Kourafalou, V.H., Oey, L.-Y., Wang, J.D., Lee, T.L., 1996. The fate of river discharge on the continental shelf. 1: modeling the river plume and the inner shelf coastal current. Journal of Geophysical Research 101, 3415–3434.

Kundu, P.K., 1976. An analysis of inertial oscillations observed near the Oregon coast. Journal of the Physical Oceanography 6, 879–893.

Li, Z., Weisberg, R.H., 1999a. West Florida continental shelf response to upwelling favorable wind forcing, part II: kinematic description. Journal of Geophysical Research 104, 13507–13527.

Li, Z., Weisberg, R.H., 1999b. West Florida continental shelf response to upwelling favorable wind forcing, part II: dynamical analyses. Journal of Geophysical Research 104, 23427–23442.

Marmorino, G.O., 1983a. Variability of current, temperature, and bottom pressure across the West Florida continental shelf, winter 1981–1982. Jounal of Geophysical Research 88 (c7), 4439–4457.

Marmorino, G.O, 1983b. Summertime coastal currents in the Northeastern Gulf of Mexico. Journal of the Physical Oceanography 13, 65–77.

Mellor, G.L., Yamada, T., 1974. A hierarchy of turbulence closure models for planetary boundary layers. J. Atmos. Sci. 13, 1791–1806.

Mellor, G.L., Yamada, T., 1982. Development of a turbulence closure model for geophysical fluid problems. Rev. Geophys. 20, 851–875.

Mitchum, T.G., Clarke, A.J., 1986a. Evaluation of frictional, wind forced long wave theory on the West Florida shelf. Journal of the Physical Oceanography 16, 1029–1037.

Mitchum, T.G., Clarke, A.J., 1986b. The frictional nearshore response to forcing by synoptic scale winds. Journal of the Physical Oceanography 16, 934–946.

Mitchum, T.G., Sturges, W., 1982. Wind-driven currents on the West Florida shelf. Journal of the Physical Oceanography 12, 1310–1317.

Morey, S.L., 1999. The spring transition of thermal stratification on a mid-latitude continental shelf. Ph.D. Dissertation, COAPS, Florida State University, Tallahassee.

Niiler, P.P., 1976. Observations of low-frequency currents on the West Florida continental shelf. Memoires Societe Royale des Sciences de Liege 6 (X), 331–358.

Orlanski, I., 1976. A simple boundary condition for unbounded hyperbolic flows. Journal of Computational Physics 21, 251–269.

Paluszkiewicz, T., Atkinson, L., Parmentier, E.S., McClain, C.R., 1983. Observation of a loop current frontal eddy intrusion onto the West Florida shelf. Journal of Geophysical Research 88, 9639–9651.

Price, J.F., 1976. Several aspects of the response of shelf waters to a cold front passage. Memoires Societe Royale des Sciences de Leige 6 (X), 201–208.

Pullen, J.D., 2000. Modeling studies of the coastal circulation off northern California, Ph.D. Dissertation, Oregon State University.

Smagorinsky, J., 1963. General circulation experiments with primitive equations. I. The basic experiment. Monthly Weather Review 91, 99–164.

Steidinger, K.A., 1983. A re-evaluation for toxic dinoflagellate biology and ecology. Progress of Phycological Research 2, 147–188.

Sturges, W., Leben, R., 2000. Frequency of ring separations from the Loop Current in the Gulf of Mexico: a revised estimate. Journal of Physical Oceanography 30, 1814–1819.

Tolbert, W.H., Salsmann, 1964. Surface circulation of the eastern Gulf of Mexico as determined by drifter bottle studies. Journal of Geophysical Research 69, 223–230.

Vargo, G.A., Carder, K.L., Gregg, W., Shanley, E., Heil, C., 1987. The potential contribution of primary production by red tides to the West Florida shelf ecosystem. Limnology and Oceanography 32, 762–767.

Weisberg, R.H., Black, B.D., Yang, H., 1996. Seasonal modulation of the west florida continental shelf circulation. Geophysical Research Letters 23, 2247–2250.

Weisberg, R.H., Black, B.D., Li, Z., 2000. A upwelling case study on the Florida's west coast. Journal of Geophysical Research 105, 11459–11469.

Weisberg, R.H., Li, Z., Muller-Karger, F., 2001. West Florida shelf response to local wind forcing, April 1998. Journal of Geophysical Research 106, C12, 31239–31262.

Williams, J., Grey, W.F., Murphy, E.B., Crane, J.J., 1977. Memoirs of the Hourglass cruise. Report of the Marine Research Laboratory, Florida of National Research, St. Petersburg, IV Part III, 134 pp.

Yang, H., Weisberg, R.H., 1999. Response of the West-Florida continental shelf to climatological monthly mean wind forcing. Journal of Geophysical Research 104, 5301–5320.

Yang, H., Weisberg, R.H., Niiler, P.P., Sturges, W., Johnson, W., 1999. Lagrangian circulation and forbidden zone on the West Florida shelf. Continental Shelf Research 19, 1221–1245.